ROYAL INSTITUTE
OF TECHNOLOGY

Exciton-plasmon interactions in semiconductor-metal nanostructures

STAFFAN HELLSTRÖM

Doctoral Thesis
Stockholm, Sweden 2012

TRITA-BIO Report 2012:4
ISSN: 1654-2312
ISBN: 978-91-7501-301-5

KTH
SE-100 44 Stockholm
SWEDEN

Akademisk avhandling som med tillstånd av Kungl Tekniska högskolan framlägges till offentlig granskning för avläggande av Teknologie Doktorsexamen i Teoretisk Kemi och Biologi 26 april 2012 i B2, Brinellvägen 23, Stockholm.

Tryck: Universitetsservice US AB

Abstract

Semiconductor quantum dots and metal nanoparticles feature very strong light-matter interactions, which has led to their use in many photonic applications such as photodetectors, biosensors, components for telecommunications etc. Under illumination both structures exhibit collective electron-photon resonances, described in the frameworks of quasiparticles as exciton-polaritons for semiconductors and surface plasmon-polaritons for metals.

To date these two approaches to controlling light interactions have usually been treated separately, with just a few simple attempts to consider exciton-plasmon interactions in a system consisting of both semiconductor and metal nanostructures.

In this work, the exciton-polaritons and surface plasmon-polaritons are first considered separately, and then combined using the Finite Difference Time Domain numerical method coupled with a master equation for the exciton-polariton population dynamics.

To better understand the properties of excitons and plasmons, each quasiparticle is used to investigate two open questions - the source of the Stokes shift between the absorption and luminescence peaks in quantum dots, and the source of the photocurrent increase in quantum dot infrared photodetectors coated by a thin metal film with holes.

The combined numerical method is then used to study a system consisting of multiple metal nanoparticles close to a quantum dot, a system which has been predicted to exhibit quantum dot-induced transparency, but is demonstrated to just have a weak dip in the absorption.

Preface

The wor presented in this thesis has been carried out at the Department of Theoretical Chemistry, School of Biotechnology, Royal Institute of Technology, Stockholm, Sweden.

List of papers included in the thesis

Paper I Z.-H. Chen, S. Hellström, Z.-J. Ning, Z.-Y. Yu, Y. Fu, *"Exciton Polariton Contribution to the Stokes Shift in Colloidal Quantum Dots"*
J. Phys. Chem. C 115, 5286 (2011)
Paper II S. Hellström, Y. Fu, *"Dynamic optical response of an excitonic quantum dot studied by solving the self-consistent Maxwell-Schrödinger equations nonperturbatively"*
Phys. Rev. B. 82, 245305 (2010)
Paper III S. Hellström, Z.-H. Chen, Y. Fu, M. Qiu, R. Soltanmoradi, Q. Wang and J. Y. Andersson *"Increased photocurrent in quantum dot infrared photodetector by subwavelength hole array in metal thin film"*
Appl. Phys. Lett. 96, 231110 (2010)
Paper IV Z.-H. Chen, S. Hellström, Z.-Y. Yu, M. Qiu, Y. Fu, *"Time-resolved photocurrents in quantum well/dot infrared photodetectors with different optical coupling structures"*
Appl. Phys. Lett. 100, 043502 (2012)
Paper V S. Hellström, Y. Fu, *"Enhanced electromagnetic field transfer across semiconductor-and-metal-nanoparticle oligomeric planar structure through exciton-plasmon interactions"*
To be published

List of papers that are not included in the thesis

Paper VI Y. Fu, S. Hellström and H. Ågren, *"Nonlinear Optical Properties of Quantum Dots - Excitons in Nanostructures"*
J. Nonlinear Optical Physics & Materials 18, 195, (2009)
Paper VII Z.-H. Chen, S. Hellström, Z.-Y. Yu, Y. Fu, *"Comb-shaped photonic crystal structure for efficient broadband light diffraction and funneling in solar cells"*
Sol. Energy Mater. Sol. Cells 99, 316 (2012)

My contribution to the papers

- I initiated the research topics and was the main writer for papers II and III, and participated in discussions and the writing of all the other papers.
- I performed the numerical calculations for papers II,III and V, and assisted in the calculational work of paper I
- I performed all the programming work for papers II,III and V

Acknowledgements

I would like to express my sincere gratitude to my supervisor, Dr. Ying Fu, for guiding me into the exciting field of quantum dot photonics and sharing his wealth of knowledge.

A special thanks goes to Prof. Hans Ågren for creating such a nice work environment and making it possible for me to work in the group.

Further, I'd like to thank Zhihui Chen for the good collaboration and all the discussions, which have led to a better understanding of the QD and plasmon physics described in this thesis.

I'd also like to thank my colleague Zhijun Ning for performing valuable experimental work in our collaboration and for discussions on growth of colloidal QDs.

I would not have been able to produce this thesis without the knowledge gained during the undergraduate and graduate education, which has been made possible thanks to my sign language interpreters.

Had I not been contacted by Linda Höglund for performing master thesis work under the supervision of Dr. Ying Fu, I would never have learned about the wonderful world of quantum dots nor would I have found the opportunity to do research in this interesting field - so a special thanks goes to her.

Last but not least, I'd like to express a heartful thanks to my family, for their patience and unconditional support.

Contents

Chapter 1

Introduction

Light is an integral part of how we perceive our environment - the interaction of light with matter can tell us a great deal about the objects around us - their color, texture, what they are made of, whether they are wet or not, and so on.

Our intuition of how light behaves breaks down when we consider nanostructured materials with features that are of similar or smaller size compared to the light's wavelength. In this regime, wave mechanics play a large role, often described by the theory of diffraction [1].

The complex interplay of optically active nanostructures and light can lead to surprising phenomena like transparency cloaks [2][3] and left-handed materials that show negative index of refraction [4].

Metallic structures exhibit strong enhancements in electromagnetic field intensities close to the surface and resonances highly sensitive to the environment, while semiconductor nanostructures have good light gathering, luminescence and long-lived dipoles that modifies the optical properties of the nanostructure. Using both materials in the same system could lead to strongly enhanced sensitivity in sensors.

Of particular interest is the use of *nanoparticles* - particles sized roughly $10^{-9} - 10^{-7}$ m. The minuscule size is much smaller than the wavelength of light, which causes the scattering and absorption properties to be very strongly dependent on the light's wavelength and the material properties. In semiconductor materials, quantum effects play a large role in determining the optical properties.

This thesis first treats the two different approaches to light-matter interaction separately in chapters 2-4, then in chapter 5 the numerical method for calculating electromagnetic fields in arbitrary structures, used in all articles included in this thesis, is described. Finally in chapter 6, the two different approaches are merged by the means of the numerical method in chapter 5, and the exciton-plasmon interactions that appear then are discussed.

Chapter 2

Semiconductor nanostructures

This chapter serves as a qualitative introduction to semiconductors and low-dimensional structures, in particular quantum dots. The concepts of *excitons* and *exciton-polaritons* in quantum dots are introduced in the next chapter, building on the general concepts established in this chapter, giving us a quantitative description that can be used to calculate electronic and optical properties of quantum dots.

2.1 Basic semiconductor theory

A simple way to categorise materials in the world around us is to investigate their conductivity which allows us to classify materials as either insulators or metals. Semiconductors have a conductivity somewhere in between, which can be tuned either in the manufacturing process or at any time.

This real-time tunability is the basic idea of the transistor, which is the main workhorse in the computing and information technology revolution that has shaped our modern world.

The optical properties of a material also depend on the conductivity, so the intermediate nature of semiconductors makes them very interesting materials for optical processes. Before we can treat the optical properties of semiconductor low-dimensional structures, some basic bulk band theory is necessary.

The average positions of the electrons of a single atom are given by the solution of the Schrödinger equation of the composite nucleus-electron system. The solutions are a set of discrete energy levels and corresponding orbitals which determine the average positions of the electrons. When considering two atoms well separated from each other, the solution is a duplicate of the first atom's energies and orbitals.

Solving the Schrödinger equation for two atoms well separated from each other gives energy levels that are identical to the one-atom case but repeated twice - the energy levels are *degenerate*. As the distance between the atoms decreases, the electrons will interact with each other which lifts the degeneracy - the degenerate electron levels will split into two levels - the strength of the splitting increases as

the distance between the atoms is decreased. Electrons in high-lying states are less localised to the atoms, so the splitting will be stronger compared to the electrons close to the nucleus.

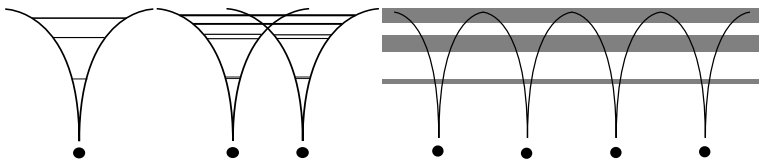

(a) One atom (b) Two atoms (c) Many atoms

Figure 2.1: Illustration of the forming of bands

As the number of atoms considered grows, so does the number of splits. Bringing N atoms close to each other leads to N splits. In real materials the number of atoms is very high, so the distance between the energy levels will be so small that we can treat the set of energy levels as a continuous range of energies - a *band*.

The range a band occupies can be seen as a range of allowed energies, while no electrons will have an energy that lies outside of the bands so the regions not within a band is called *forbidden*. Just solving the Schrödinger equations gives us all possible solutions, of which there are many more than available electrons in the system, so the highest filled band, the *valence* band, and the empty band above it, the *conduction* band are of particular interest.

In metals there is no gap between the valence and conduction bands - electrons are free to increase their energy and enter the conduction band where they can freely move around in space. In insulators the energy difference, the *bandgap* between the valence and conduction bands is high enough so that electrons cannot change bands easily.

By choosing appropriate semiconductor material alloys it is possible to control the bandgap. Of particular interest is when the bandgap lies between 0.1 and 4 eV, which makes it possible for electrons to be excited by near-UV, visible light and infrared radiation. The physical processes caused by excitations makes semiconductors good materials for optical devices.

As most semiconductor materials are crystalline, the atoms are ordered in a periodic crystal lattice. The periodic potential of the atoms strongly influences the wavefunctions of the electrons - the classic way to treat this is to separate the wavefunction in two parts, one rapidly changing and a more smooth function, the *envelope function*.

For an uniform sample, we can use the Bloch theorem to write out the wavefunction for a free electron in a semiconductor:

$$\psi_{n\boldsymbol{k}}(\boldsymbol{r}) = e^{i\boldsymbol{k}\cdot\boldsymbol{r}} u_{n\boldsymbol{k}}(\boldsymbol{r})$$
$$u_{n\boldsymbol{k}}(\boldsymbol{r}) = u_{n\boldsymbol{k}}(\boldsymbol{r} + \boldsymbol{R})$$

The index n picks the electron state, $\boldsymbol{r}$ is the position of the electron in space, $\boldsymbol{R}$ is the lattice period, and the crystal wavevector $\boldsymbol{k}$ has the relationship with the wavelength: $|\boldsymbol{k}| = \frac{2\pi}{\lambda}$.

The details of the semiconductor material is hidden in the rapidly varying *periodic Bloch function* $u_{n\boldsymbol{k}}$ which has the periodicity of the atomic lattice.

2.2 Effective mass

The electrons moving in the lattice are strongly influenced by the periodic atomic potentials - in order to describe the change in electron velocity we use the concept of an *effective mass* of the electron inside a particular semiconductor material.

An electron whose energy dependence on crystal momentum $\hbar\boldsymbol{k}$ can be described by the dispersion relation $E(\boldsymbol{k})$ has the group velocity

$$\boldsymbol{v} = \frac{1}{\hbar}\frac{\mathrm{d}E(\boldsymbol{k})}{\mathrm{d}\boldsymbol{k}} \tag{2.1}$$

The momentum $\boldsymbol{p} = m\boldsymbol{v}$ can also be expressed as $\boldsymbol{p} = \hbar\boldsymbol{k}$. Using Newton's second law, $\boldsymbol{F} = m\boldsymbol{a}$:

$$\begin{aligned}\hbar\frac{\mathrm{d}\boldsymbol{k}}{\mathrm{d}t} =& m\frac{\mathrm{d}\boldsymbol{v}}{\mathrm{d}t}\\ =& \frac{m}{\hbar}\frac{\mathrm{d}^2E(\boldsymbol{k})}{\mathrm{d}t\,\mathrm{d}\boldsymbol{k}}\\ =& \frac{m}{\hbar}\frac{\mathrm{d}^2E(\boldsymbol{k})}{\mathrm{d}\boldsymbol{k}^2}\frac{\mathrm{d}\boldsymbol{k}}{\mathrm{d}t}\end{aligned} \tag{2.2}$$

From this we can obtain a mass which depends on the energy dispersion:

$$\frac{1}{m^*} = \frac{1}{\hbar^2}\frac{\mathrm{d}^2E(\boldsymbol{k})}{\mathrm{d}\boldsymbol{k}^2} \tag{2.3}$$

Using effective masses is a rough approximation but still very efficient and considering the multitude of other possible differences between a model and reality, the effective mass approximation is a very effective and acceptable approximation.

The effective mass approximation is used throughout this thesis. There are more accurate methods available, such as the $\boldsymbol{k}\cdot\boldsymbol{p}$ method by Kane [5], which takes the effects of multiple bands into account, or the pseudopotential method [6] which consider individual atoms and is therefore more accurate at a great computational cost. However, these methods often introduce considerable complexity and calculational cost, or require material parameters that are difficult to measure or calculate.

2.3 Nanostructures

For a nonuniform sample, both the envelope function and the Bloch function will vary in space. Of particular interest are the cases of reduced dimensionality -

systems with variation of material composition in one or more axes and no change in material along the other axes.

By choosing appropriate combinations of materials with different bandgaps and positions of valence and conduction bands, it is possible to design sophisticated semiconductor heterostructures.

A thin planar layer of a semiconductor material with a small bandgap embedded inside a bulk material with larger bandgap (or an insulator) is called a *Quantum Well*. For a quantum well we can use the bulk description along two axes but along the third axis the envelope function needs to be changed significantly. This leads to a confinement of electrons in the third axis if the electron's energy is not sufficiently high to escape the quantum well, while the electron is free to move along the two other axes.

The confinement along the third axis causes *quantization* of the energy spectrum of the electrons.

Quantum wires have confinement in two axes. Often real quantum wires are not infinite in extent along the extended axis but are still sufficiently long that a nearly bulklike treatment of the electrons is possible along that axis.

Quantum dots have confinement in all the three axes, so the electrons inside are not free to move anywhere and the energy spectrum is completely quantized.

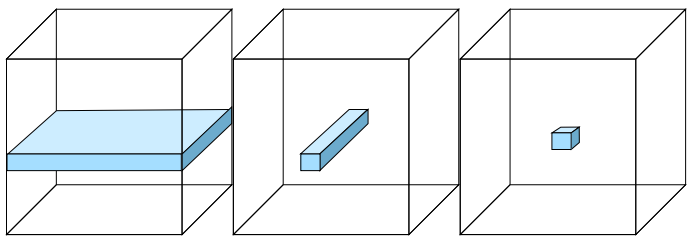

(a) Quantum well (b) Quantum wire (c) Quantum dot

Figure 2.2: Dimensional reduction of nanostructures

The different quantizations of energy depending on dimensionality affect the electron density of states (DOS) - the number N of allowed electron energy levels in an energy interval around an energy E, $D(E) = dN(E)/dE$.

In bulk the DOS, using the effective mass m^* to characterize the material, is given by

$$D_{3D}(E) = \frac{1}{2\pi^2}\left(\frac{2m^*}{\hbar^2}\right)^{3/2}\sqrt{E}\Theta(E) \tag{2.4}$$

For quantum wells:

$$D_{2D}(E) = \sum_n \frac{m^*}{\pi\hbar^2}\Theta(E - E_n) \tag{2.5}$$

where E_n indicates the quantized energy levels. The Heaviside function $\Theta(E - E_n)$ is zero for $E < E_n$ and one for $E \geq E_n$.

For quantum wires:

$$D_{1D}(E) = \sum_n \frac{1}{\pi\hbar}\sqrt{\frac{2m^*}{E - E_n}}\Theta(E - E_n) \tag{2.6}$$

Quantum dots (QDs) have no $\boldsymbol{k}-$dependence at all, which means the energy levels are completely discretized:

$$D_{0D}(E) = \sum_n 2\delta(E - E_n) \tag{2.7}$$

The factor 2 comes from the spin-multiplicity, as two electrons are allowed in each energy level. The discrete levels are why quantum dots are sometimes called "artificial atoms". The energy levels of a quantum dot depends strongly on the size of the QD, allowing for great flexibility in designing the absorption and luminescence of a material consisting of QDs.

The densities of states are sketched in figure 2.3.

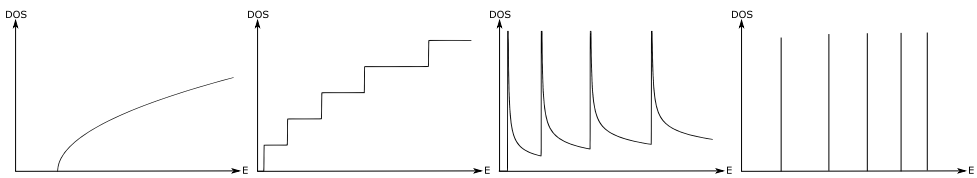

(a) 3D (b) 2D (c) 1D (d) 0D

Figure 2.3: Densities of States for various dimensions

2.4 Quantum dots

Typically quantum dots have sizes of around 0.5-50 nm, depending on the manufacturing method. Epitaxial methods, where the dots are formed by nucleation of adsorbed thin films due to strain mismatch between the dot and host materials, lead to roughly hemispherical or pyramidal quantum dots embedded in a host semiconductor material. This type of dots can have quite large bases but small heights, less than 10 nm.

Colloidal manufacturing methods, where the dots are grown by crystallization of the constituent atoms into spheroids, create very small dots in a liquid solution. This type of QDs are often used in chemical sensors and biosensors, utilizing different surface coatings that can bind to target molecules [12].

In real ensembles of quantum dots, the sharp delta functions are smoothed due to size variation of the QDs and also due to electron-phonon interactions. In general the absorption spectrum will be quite smooth with a few peaks.

Typical absorption and luminescence for two quantum dots with different sizes are shown in fig. 2.4, where a difference in the peak absorption and luminescence can be seen. This is the *Stokes shift*. There are many suggested sources for this effect [7, 8, 9, 10, 11], usually focusing on variations in the bandstructure leading to optically inactive ground states so that absorption is shifted. In paper I, we proposed another possible source for the Stokes shift, due to the exciton-polariton effect [13] which is discussed in further detail in chapter 3.4.

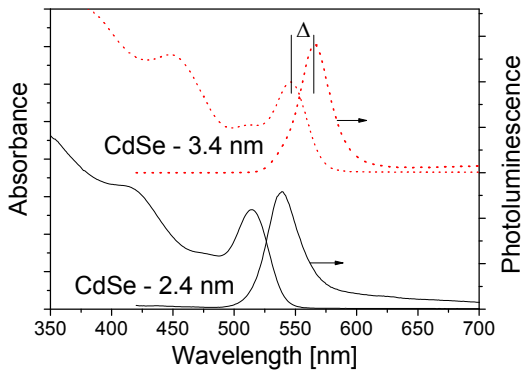

Figure 2.4: Absorption and photoluminescence for two quantum dots. The larger QD's values have been shifted upwards for clarity.

Colloidal quantum dots exhibit a blinking effect, where the luminescence of a quantum dot can be observed to cease for a relatively long time (up to a few seconds) at random intervals. The reasons for this effect is still under debate, but the absorption and polarization properties are believed to not be affected [14] so the structures under investigation here are not negatively impacted.

An important advantage of semiconductor quantum dots over dye molecules such as Rhodamine-3G is that the absorption spectrum is much broader for QDs as photons of many energy levels larger than the bandgap energy will be absorbed like in figure 2.4, unlike the dye molecule which will only absorb a narrow range of energies. This is especially important in solar cell applications, which depend on absorbing a wide range of energies from the solar blackbody spectrum.

Chapter 3

Exciton-Polaritons

The optical properties of most materials are strongly influenced by electron excitations so to be able to describe quantitatively the optical properties of a quantum dot a model of the electron dynamics in the quantum dot is needed. This chapter introduces the idea of *excitons* - pairs of excited electrons in the conduction band and the holes in the valence band the excited electron leaves. The energy is briefly considered but the main emphasis lies on obtaining the spatial distribution of the exciton in a model quantum dot, the photodynamics of the exciton population, and the polarization which is the basis for most measurable optical properties.

3.1 Excitons

When a photon has an energy larger than the bandgap, it can excite an electron from the valence band in a semiconductor into the conduction band. The freed state in the valence band is often treated as a particle, a "hole", with its own mass, positive charge, and ability to interact with other electrons and holes. The hole does not exist *per se* but the interactions with valence electrons around the hole is equivalent to interacting with just the hole if the hole's properties are properly modeled, for example by having a different effective mass for the holes.

An electron-hole pair can become bound to each other by the Coulomb attraction between the differently charged particles. The full Hamiltonian of a system consisting of an electron at position $\boldsymbol{r}_e$ and a hole at $\boldsymbol{r}_h$ in a QD with dielectric constant ε:

$$H = -\frac{\hbar^2\nabla_e^2}{2m_0} + U(\boldsymbol{r}_e) - \frac{\hbar^2\nabla_h^2}{2m_0} + U(\boldsymbol{r}_h) - \frac{e^2}{4\pi\varepsilon|\boldsymbol{r}_e - \boldsymbol{r}_h|} \tag{3.1}$$

The potential $U(\boldsymbol{r}_{e,h})$ is the actual atomic potential, not the effective-mass potential $V(\boldsymbol{r})$ which makes obtaining a solution rather complicated. Another difficulty is that the last term, which represents the Coulomb interaction, prevents

us from constructing an eigenstate as the simple product of an electron and a hole wavefunction, $\psi_{c\boldsymbol{k}_e}(\boldsymbol{r}_e)\psi_{v\boldsymbol{k}_h}(\boldsymbol{r}_h)$.

To get around these complications, a linear combination of multiple electron-hole states has to be used. Let the wavevector of the combined electron-hole state be $\boldsymbol{K} = \boldsymbol{k}_e + \boldsymbol{k}_h$, and use $c(v)$ to denote conduction(valence) bands.

$$\Psi_{n\boldsymbol{K}}(\boldsymbol{r}_e, \boldsymbol{r}_h) = \sum_{c\boldsymbol{k}_e, v\boldsymbol{k}_h} A_{n\boldsymbol{K}}(c\boldsymbol{k}_e, v\boldsymbol{k}_h)\psi_{c\boldsymbol{k}_e}(\boldsymbol{r}_e)\psi_{v\boldsymbol{k}_h}(\boldsymbol{r}_h) \tag{3.2}$$

where the electron and hole states are represented as Bloch functions:

$$\psi_{c\boldsymbol{k}}(\boldsymbol{r}) = \frac{1}{\sqrt{\Omega}} e^{i\boldsymbol{k}\cdot\boldsymbol{r}} u_{c\boldsymbol{k}}(\boldsymbol{r})\,; \qquad \psi_{v\boldsymbol{k}}(\boldsymbol{r}) = \frac{1}{\sqrt{\Omega}} e^{-i\boldsymbol{k}\cdot\boldsymbol{r}} u_{v\boldsymbol{k}}(\boldsymbol{r}) \tag{3.3}$$

where Ω is the lattice volume.

If the exchange interaction between the electron and hole can be ignored then the exciton state and its energy E, defined as the difference from the ground state, can be obtained by solving the equation system

$$\begin{aligned} &\left[E - E_c(\boldsymbol{k}_e) + E_v(\boldsymbol{k}_h)\right] A_{n\boldsymbol{K}}(c\boldsymbol{k}_e, v\boldsymbol{k}_h) = \\ &\sum_{c\boldsymbol{k}'_e, v\boldsymbol{k}'_h} \langle c\boldsymbol{k}_e, v\boldsymbol{k}_h | V(\boldsymbol{r}_e - \boldsymbol{r}_h) | c\boldsymbol{k}'_e, v\boldsymbol{k}'_h \rangle A_{n\boldsymbol{K}}(c\boldsymbol{k}_e, v\boldsymbol{k}_h) \end{aligned} \tag{3.4}$$

where $E_c(\boldsymbol{k}_e)$ and $E_v(\boldsymbol{k}_h)$ are single-electron(hole) conduction- and valence-band energies.

An effective-mass approximation to the solution of this is obtained from solving the simplified differential equation [16][17]

$$\left[E_c(-i\nabla_e) - E_v(-i\nabla_h) + V(\boldsymbol{r}_e - \boldsymbol{r}_h)\right] \psi_{n\boldsymbol{K}}(\boldsymbol{r}_e, \boldsymbol{r}_h) = E\psi_{n\boldsymbol{K}}(\boldsymbol{r}_e, \boldsymbol{r}_h) \tag{3.5}$$

Here $E_c(-i\nabla_e)$ and $E_v(-i\nabla_h)$ are power series expressions of the single-electron (hole) energies in the conduction(valence) bands, but expanded in a power series with $-i\nabla_e$ used instead of $\boldsymbol{k}_e$.

The solution to this differential equation, $\psi_{n\boldsymbol{K}}(\boldsymbol{r}_e, \boldsymbol{r}_h)$ is the exciton *envelope function*. The actual wavefunction contains the Bloch periodic functions,

$$\Psi_{n\boldsymbol{K}}(\boldsymbol{r}_e, \boldsymbol{r}_h) = \Omega\psi_{n\boldsymbol{K}}(\boldsymbol{r}_e, \boldsymbol{r}_h) u_c(\boldsymbol{r}_e) u_v(\boldsymbol{r}_h) \tag{3.6}$$

As a special case of interest we consider colloidal quantum dots which can be approximated as spheres in vacuum - which makes it possible to obtain an analytical expression for the wavefunction. Using relative center-of-mass coordinates

$$\boldsymbol{r} = \boldsymbol{r}_e - \boldsymbol{r}_h\,,\ \boldsymbol{R} = \frac{m_e^*\boldsymbol{r}_e + m_h^*\boldsymbol{r}_h}{m_e^* + m_h^*} \tag{3.7}$$

where the reduced effective mass m_r^* is:

$$\frac{1}{m_r^*} = \frac{1}{m_e^*} - \frac{1}{m_h^*} \tag{3.8}$$

the Hamiltonian becomes

$$H = -\frac{\hbar^2}{\nabla_{\boldsymbol{R}}^2} 2(m_e^* + m_h^*) - \frac{\hbar^2 \nabla_{\boldsymbol{r}}^2}{2m_r^*} - \frac{e^2}{4\pi\varepsilon|\boldsymbol{r}|} \tag{3.9}$$

The solution to the Schrödinger equation using this Hamiltonian is the product of a wavefunction corresponding to the center-of-mass motion and the relative electron-hole overlap.

The spherically symmetric problem is trivially reduced to one dimension - the QD is then like a quantum well of width R_{QD} and infinite barriers, which has the well-known normalized solution:

$$\frac{1}{|\boldsymbol{R}|\sqrt{2\pi R_{QD}}} \sin\left(\frac{n\pi|\boldsymbol{R}|}{R_{QD}}\right) \tag{3.10}$$

The envelope function representing the exciton state, given by the overlap of the electron and hole, is:

$$\frac{1}{\sqrt{\pi a_B^3}} e^{-|\boldsymbol{r}|/a_B} \tag{3.11}$$

The exciton Bohr radius $a_B = 4\pi\varepsilon_\infty \hbar^2/m_r^* e^2$ varies between materials, and is typically around $1-5$ nm for IV-VI semiconductors and $5-40$ nm for III-V semiconductors.

Together these give the wavefunction for the ground state ($n = 1$) exciton in a spherical quantum dot:

$$\Psi(\boldsymbol{r}_e, \boldsymbol{r}_h) = \frac{1}{|\boldsymbol{R}|\sqrt{2\pi R_{QD}}} \sin\left(\frac{\pi|\boldsymbol{R}|}{R_{QD}}\right) \frac{1}{\sqrt{\pi a_B^3}} e^{-|\boldsymbol{r}_e - \boldsymbol{r}_h|/a_B} u_c(\boldsymbol{r}_e) u_v(\boldsymbol{r}_h) \tag{3.12}$$

It should be noted that the approximations used in this chapter are only valid for quantum dots with radii smaller than or similar to the exciton Bohr radius. Quantum dots with sizes larger than the exciton Bohr radius will not display size-dependent energy levels and will converge towards bulk properties.

The corresponding exciton binding energy, for QDs smaller than the exciton Bohr radius, is given by

$$E_n = -\frac{m_r^* e^4}{2\varepsilon^2 h^2 n^2} \tag{3.13}$$

The negative value indicates the bound nature of the exciton - the exciton configuration is by nature preferred compared to that of a free electron-hole pair in a quantum dot.

3.2 Exciton dynamics and optical properties

Knowing the electronic structure, now the optical properties are discussed, using time-dependent theory.

Of central importance is the study of the polarization, which in turn determines several other optical properties such as the dielectric constant, by $\boldsymbol{D} = \varepsilon \boldsymbol{E} = \varepsilon_0 \boldsymbol{E} + \boldsymbol{P}$, where $\boldsymbol{P}$ is a linear function of $\boldsymbol{E}$.

The polarization can be seen as the expectation value of the electric dipole $\boldsymbol{d}(\boldsymbol{r}) = -e\boldsymbol{r}$:

$$\boldsymbol{P}(\boldsymbol{r}, t) = \langle \boldsymbol{r}_e, \boldsymbol{r}_h, t | \boldsymbol{d}(\boldsymbol{r}) | \boldsymbol{r}_e, \boldsymbol{r}_h, t \rangle \tag{3.14}$$

If it is assumed that the electromagnetic fields are of moderate strength so that they do not perturb the spatial distribution of the exciton, then the time-dependent wavefunctions is a product of the occupation probability and the spatial distribution which was obtained in the previous section:

$$|\boldsymbol{r}_e, \boldsymbol{r}_h, t\rangle = c_0(t)|\Psi_0(\boldsymbol{r}_e, \boldsymbol{r}_h)\rangle + \sum_{n\boldsymbol{K}} c_{n\boldsymbol{K}}(t)|\Psi_{n\boldsymbol{K}}(\boldsymbol{r}_e, \boldsymbol{r}_h, t)\rangle \tag{3.15}$$

where $\Psi_{n\boldsymbol{K}}(\boldsymbol{r}_e, \boldsymbol{r}_h, t) = \Psi_{n\boldsymbol{K}}(\boldsymbol{r}_e, \boldsymbol{r}_h) e^{-i\omega_{n\boldsymbol{K}} t}$. The zero indices in $c_0(t)$ and Ψ_0 signify the unexcited vacuum state without any excitons. The exciton resonance frequency $\omega_{n\boldsymbol{K}}$ is given by $E_g + E_c + E_v + E_n$, i.e. the difference between the electron and hole energies when exciton binding is taken into account - E_g is here the bandgap energy, E_c the energy of the electron relative to the bottom of the conduction band, E_v the energy of the hole relative to the top of the valence band, and E_n is the exciton binding energy.

We limit our discussion to the polarization due to transitions between excited states and the empty ground state Ψ_0, which can be expected to be the most common kind of transition [15]. Furthermore, we only consider direct bandgap semiconductors and no phonon effects, so the momentum $\boldsymbol{k}$ should remain the same.

The time-dependent Schrödinger equation then becomes:

$$i\hbar \frac{\partial |\boldsymbol{r}_e, \boldsymbol{r}_h, t\rangle}{\partial t} = (H_0 + H_1)|\boldsymbol{r}_e, \boldsymbol{r}_h, t\rangle \tag{3.16}$$

where the energy Hamiltonian H_0 is the identical to (3.9), which doesn't need to be evaluated directly if the energies are known beforehand. In that case, $H_0 \Psi_{n\boldsymbol{K}} = \hbar\omega_{n\boldsymbol{K}} \Psi_{n\boldsymbol{K}}$. For the ground unexcited state the value of ω_0 can be set to zero.

The perturbation Hamiltonian, which represents the effect by electromagnetic fields on the exciton, is:

$$H_1 = \int \boldsymbol{d}(\boldsymbol{r}) \cdot \boldsymbol{E}(\boldsymbol{r}, t)\, \mathrm{d}\boldsymbol{r} \tag{3.17}$$

where $\boldsymbol{d}(\boldsymbol{r})$ is the dipole moment operator

$$\boldsymbol{d}(\boldsymbol{r}) = -e\boldsymbol{r}_e \delta(\boldsymbol{r} - \boldsymbol{r}_e) + e\boldsymbol{r}_h \delta(\boldsymbol{r} - \boldsymbol{r}_h) \tag{3.18}$$

A straightforward first-order approximation to the time-dependent Schrödinger equation is:

$$i\hbar\frac{dc_{n\boldsymbol{K}}(t)}{dt} = c_0(t)\langle\Psi_{n\boldsymbol{K}}(\boldsymbol{r}_e,\boldsymbol{r}_h)|\int \boldsymbol{d}(\boldsymbol{r})\cdot\boldsymbol{E}(\boldsymbol{r},t)\,\mathrm{d}\boldsymbol{r}|\Psi_0(\boldsymbol{r}_e,\boldsymbol{r}_h)\rangle e^{i\omega_{n\boldsymbol{K}}t} \tag{3.19}$$

where the other terms were cancelled out due to symmetry:

$$\langle\Psi_{n\boldsymbol{K}}(\boldsymbol{r}_e,\boldsymbol{r}_h)|\int \boldsymbol{d}(\boldsymbol{r})\cdot\boldsymbol{E}(\boldsymbol{r},t)\,\mathrm{d}\boldsymbol{r}|\Psi_{n\boldsymbol{K}}(\boldsymbol{r}_e,\boldsymbol{r}_h)\rangle = 0 \tag{3.20}$$

Solving this will yield the population variation over time due to the excitation by the electromagnetic field $\boldsymbol{E}(\boldsymbol{r},t)$. A steady-state solution can be obtained by using a continuous-wave excitation $\boldsymbol{E}(\boldsymbol{r},t) = \boldsymbol{E}(\boldsymbol{r},\omega)e^{-i\omega t} + c.c$, where $c.c.$ denotes the complex conjugate.

This gives the solution

$$c_{n\boldsymbol{K}}(t) = \frac{e^{i(\omega_{n\boldsymbol{K}}-\omega)t}}{\hbar(\omega_{n\boldsymbol{K}}-\omega)}\langle\Psi_{n\boldsymbol{K}}(\boldsymbol{r}_e,\boldsymbol{r}_h)|\int \boldsymbol{d}(\boldsymbol{r})\cdot\boldsymbol{E}(\boldsymbol{r},\omega)\,\mathrm{d}\boldsymbol{r}|\Psi_0(\boldsymbol{r}_e,\boldsymbol{r}_h)\rangle \tag{3.21}$$

Here the dipole matrix element is

$$\begin{aligned}&\langle\Psi_{n\boldsymbol{K}}(\boldsymbol{r}_e,\boldsymbol{r}_h)|\int \boldsymbol{d}(\boldsymbol{r})\cdot\boldsymbol{E}(\boldsymbol{r},t)\,\mathrm{d}\boldsymbol{r}|\Psi_0(\boldsymbol{r}_e,\boldsymbol{r}_h)\rangle\\ =&\langle\Psi_{n\boldsymbol{K}}(\boldsymbol{r}_e,\boldsymbol{r}_h)|\int e\boldsymbol{r}_e\delta(\boldsymbol{r}-\boldsymbol{r}_e)\cdot\boldsymbol{E}(\boldsymbol{r},t)\,\mathrm{d}\boldsymbol{r}|\Psi_0(\boldsymbol{r}_e,\boldsymbol{r}_h)\rangle\end{aligned} \tag{3.22}$$

which will be evaluated, using a second-quantisation approach similar to that of [18].

First the position basis is changed to momentum basis by:

$$\langle\Psi_{n\boldsymbol{K}}(\boldsymbol{r}_e,\boldsymbol{r}_h)|\boldsymbol{r}|\Psi_0(\boldsymbol{r}_e,\boldsymbol{r}_h)\rangle = \frac{1}{im_0\omega_n}\langle\Psi_{n\boldsymbol{K}}(\boldsymbol{r}_e,\boldsymbol{r}_h)|\boldsymbol{p}|\Psi_0(\boldsymbol{r}_e,\boldsymbol{r}_h)\rangle \tag{3.23}$$

The polarization operator creates an electron and a hole, here expressed in second-quantization formalism:

$$\boldsymbol{p} = \sum_{\boldsymbol{k}_e,\boldsymbol{k}_h} a^\dagger_{\boldsymbol{k}_e} b^\dagger_{\boldsymbol{k}_h}\langle c\boldsymbol{k}_e|\boldsymbol{p}|v\boldsymbol{k}_h\rangle \tag{3.24}$$

where $a^\dagger_{\boldsymbol{k}_e}$ adds an electron with momentum $\boldsymbol{k}_e$, and $\boldsymbol{b}^\dagger_{\boldsymbol{k}_h}$ adds a hole with momentum $\boldsymbol{k}_h$. The corresponding annihilation operators are $a_{\boldsymbol{k}_e}$ which removes an electron and $b_{\boldsymbol{k}_h}$ which removes a hole.

Using this formalism, the excited state can be constructed from the empty ground state by creating electrons and holes. The conjugate of the excited state, needed in eq. 3.23 is:

$$\langle\Psi_{n\boldsymbol{K}}(\boldsymbol{r}_e,\boldsymbol{r}_h)| = \sum_{\boldsymbol{k}_e,\boldsymbol{k}_h} A^*_{n,\boldsymbol{K}}(\boldsymbol{k}_e,\boldsymbol{k}_h)\langle\Psi_0(\boldsymbol{r}_e,\boldsymbol{r}_h)|b_{\boldsymbol{k}_h}a_{\boldsymbol{k}_e} \tag{3.25}$$

Then the momentum matrix element becomes:

$$\begin{aligned}
&\langle \Psi_{n\boldsymbol{K}}(\boldsymbol{r}_e,\boldsymbol{r}_h)| \int \boldsymbol{p}\cdot\boldsymbol{E}\,\mathrm{d}\boldsymbol{r}|\Psi_0(\boldsymbol{r}_e,\boldsymbol{r}_h)\rangle \\
&= \sum_{\boldsymbol{k}_e,\boldsymbol{k}_h} A^*_{n,\boldsymbol{K}}\langle \Psi_0(\boldsymbol{r}_e,\boldsymbol{r}_h)| \int b_{\boldsymbol{k}_h}a_{\boldsymbol{k}_e}a^\dagger_{\boldsymbol{k}_e}b^\dagger_{\boldsymbol{k}_h}\langle c\boldsymbol{k}_e|\boldsymbol{p}|v\boldsymbol{k}_h\rangle\cdot\boldsymbol{E}\,\mathrm{d}\boldsymbol{r}|\Psi_0(\boldsymbol{r}_e,\boldsymbol{r}_h)\rangle \\
&= \sum_{\boldsymbol{k}_e,\boldsymbol{k}_h} A^*_{n,\boldsymbol{K}}\langle \Psi_0(\boldsymbol{r}_e,\boldsymbol{r}_h)| \int \langle c\boldsymbol{k}_e|\boldsymbol{p}|v\boldsymbol{k}_h\rangle\cdot\boldsymbol{E}\,\mathrm{d}\boldsymbol{r}|\Psi_0(\boldsymbol{r}_e,\boldsymbol{r}_h)\rangle
\end{aligned} \tag{3.26}$$

where the reader is reminded that we only discuss excitations from the empty ground state so that the creation-annihilation pairs always return nonzero results. We have here also hidden the dirac delta used in the dipole moment operator, $\delta(\boldsymbol{r}-\boldsymbol{r}_e)$ which will be added back later.

The exciton momentum $\langle c\boldsymbol{k}_e|\boldsymbol{p}|v\boldsymbol{k}_h\rangle$ is now to be derived. It is for the general case of an exciton in a semiconductor material, not dependent on the specific geometry of our nanostructure, so we can use bulk plane wave expressions for the electron and hole wavefunctions of an excited electron with momentum $\boldsymbol{k}_e$ and an excited hole with momentum $-\boldsymbol{k}_h$:

$$|c\boldsymbol{k}_e\rangle = \frac{1}{\sqrt{\Omega}}e^{i\boldsymbol{k}_e\cdot\boldsymbol{r}}u_c(\boldsymbol{r}) \qquad |v\boldsymbol{k}_h\rangle = \frac{1}{\sqrt{\Omega}}e^{-i\boldsymbol{k}_h\cdot\boldsymbol{r}}u_v(\boldsymbol{r}) \tag{3.27}$$

Thus the momentum matrix element is:

$$\begin{aligned}
&\langle c\boldsymbol{k}_e|\boldsymbol{p}|v\boldsymbol{k}_h\rangle = \langle c\boldsymbol{k}_e|\frac{i}{\hbar}\nabla|v\boldsymbol{k}_h\rangle = \frac{i}{\hbar V}\int e^{i\boldsymbol{k}_e\cdot\boldsymbol{r}}u_c^*(\boldsymbol{r})\nabla\left(e^{-i\boldsymbol{k}_h\cdot\boldsymbol{r}}u_v(\boldsymbol{r})\right)d^3r \\
&\frac{i}{\hbar}e^{-i(\boldsymbol{k}_e+\boldsymbol{k}_h)\cdot\boldsymbol{r}}\left(i\boldsymbol{k}_h\underbrace{\langle u_c|u_v\rangle}_{=0}+\langle u_c|\nabla u_v\rangle\right) = \{\nabla=\hbar\boldsymbol{p}/i\} \\
&= e^{-i(\boldsymbol{k}_e+\boldsymbol{k}_h)\cdot\boldsymbol{r}}\langle u_c|\boldsymbol{p}|u_v\rangle \approx e^{-i(\boldsymbol{k}_e+\boldsymbol{k}_h)\cdot\boldsymbol{r}}\boldsymbol{p}_{cv}(0)
\end{aligned} \tag{3.28}$$

where we assume that the momentum is roughly constant over the small part of $\boldsymbol{k}$ space which the incoming light momentum can occupy, and label that value as $\boldsymbol{p}_{cv}(0)$. The (0) will be dropped from now on. Its value is often taken from experimental measurements and parametrized using the Kane parameter $E_P = 2m_0p_{cv}^2/\hbar^2$. Note that $\boldsymbol{p}_{cv}$ is imaginary and has an unknown direction which depends on the crystal orientation.

We thus have

$$\sum_{\boldsymbol{k}_e,\boldsymbol{k}_h} A^*_{n,\boldsymbol{K}}\langle \Psi_0(\boldsymbol{r}_e,\boldsymbol{r}_h)| \int e^{-i(\boldsymbol{k}_e+\boldsymbol{k}_h)\cdot\boldsymbol{r}}\boldsymbol{p}_{cv}\cdot\boldsymbol{E}\,\mathrm{d}\boldsymbol{r}|\Psi_0(\boldsymbol{r}_e,\boldsymbol{r}_h)\rangle \tag{3.29}$$

So if we assume that the electromagnetic wave can be written as a plane wave inside the QD, $\boldsymbol{E} = \boldsymbol{E}_{\boldsymbol{k}}e^{i\boldsymbol{k}\cdot\boldsymbol{r}}$, and that $\boldsymbol{k}_e, \boldsymbol{k}_h, \boldsymbol{k}$ all are small (so that the total

exciton-polariton momentum $\boldsymbol{k}_e + \boldsymbol{k}_h - \boldsymbol{k}$ is small too) and that the $\boldsymbol{E}$ field is slowly varying over the QD so that we can treat it as roughly constant over the QD volume, then the spatial integration can be simplified (recall that we are only integrating over the QD volume, which is usually much smaller than the wavelength of the external illumination)

The spatial integral over the exponentials vanishes or becomes very small whenever $\boldsymbol{k}_e + \boldsymbol{k}_h - \boldsymbol{k}$ is nonzero, so we can approximatively write this integral as a dirac distribution function $\delta_{\boldsymbol{k}_e+\boldsymbol{k}_h,\boldsymbol{k}}$. We have:

$$\langle \Psi_{n\boldsymbol{K}}(\boldsymbol{r}_e, \boldsymbol{r}_h) | \boldsymbol{p} \cdot \boldsymbol{E} | \Psi_0(\boldsymbol{r}_e, \boldsymbol{r}_h) \rangle = \sum_{\boldsymbol{k}_e, \boldsymbol{k}_h} A^*_{n,\boldsymbol{K}}(\boldsymbol{k}_e, \boldsymbol{k}_h) \delta_{\boldsymbol{k}_e+\boldsymbol{k}_h,\boldsymbol{k}} \boldsymbol{p}_{cv} \cdot \boldsymbol{E}_{\boldsymbol{k}} \tag{3.30}$$

As $\int e^{i(\boldsymbol{K}-\boldsymbol{k})\cdot\boldsymbol{r}} \,\mathrm{d}\boldsymbol{r} = \delta_{\boldsymbol{K},\boldsymbol{k}}$, we can regain the exact exciton wavefunction from (3.2) and use it in the expression:

$$\langle \Psi_{n\boldsymbol{K}}(\boldsymbol{r}_e, \boldsymbol{r}_h) | \int \boldsymbol{p} \cdot \boldsymbol{E} \,\mathrm{d}\boldsymbol{r} | \Psi_0(\boldsymbol{r}_e, \boldsymbol{r}_h) \rangle = \int \Psi^*_{n,\boldsymbol{K}}(\boldsymbol{r}_e, \boldsymbol{r}_h) \boldsymbol{p}_{cv} \cdot \boldsymbol{E}(\boldsymbol{r}) \,\mathrm{d}\boldsymbol{r} \tag{3.31}$$

Finally, we recall that there were two dirac delta functions in the dipole operator which were temporarily hidden. The effect of adding them back is simply changing $\boldsymbol{r}_e$ and $\boldsymbol{r}_h$ to $\boldsymbol{r}$, so the final result for the dipole matrix element is:

$$\langle \Psi_{n\boldsymbol{K}}(\boldsymbol{r}_e, \boldsymbol{r}_h) | \int \boldsymbol{d}(\boldsymbol{r}) \cdot \boldsymbol{E}(\boldsymbol{r}, t) \,\mathrm{d}\boldsymbol{r} | \Psi_0(\boldsymbol{r}_e, \boldsymbol{r}_h) \rangle = \frac{e}{i m_0 \omega_{n\boldsymbol{K}}} \boldsymbol{p}_{cv} \cdot \int \Psi^*_{n\boldsymbol{K}}(\boldsymbol{r}, \boldsymbol{r}) \boldsymbol{E}(\boldsymbol{r}) \,\mathrm{d}^3 r \tag{3.32}$$

A similar derivation yields

$$\langle \Psi_{n\boldsymbol{K}}(\boldsymbol{r}_e, \boldsymbol{r}_h) | \boldsymbol{d}(\boldsymbol{r}) | \Psi_0(\boldsymbol{r}_e, \boldsymbol{r}_h) \rangle = \frac{e}{i m_0 \omega_{n\boldsymbol{K}}} \boldsymbol{p}_{cv} \Psi^*_{n\boldsymbol{K}}(\boldsymbol{r}, \boldsymbol{r}) \tag{3.33}$$

The polarization is:

$$\begin{aligned} \boldsymbol{P}(\boldsymbol{r}, t) =& \langle \boldsymbol{r}_e, \boldsymbol{r}_h, t | \boldsymbol{d}(\boldsymbol{r}) | \boldsymbol{r}_e, \boldsymbol{r}_h, t \rangle \\ =& \langle \Psi_0(t) | \boldsymbol{d}(\boldsymbol{r}) | \Psi_{n\boldsymbol{K}}(\boldsymbol{r}_e, \boldsymbol{r}_h, t) \rangle c^*_{n\boldsymbol{K}}(t) c_0(t) + c.c. \\ =& \frac{ie}{m_0 \omega_{n\boldsymbol{K}}} \boldsymbol{p}^*_{cv} \Psi_{n\boldsymbol{K}}(\boldsymbol{r}, \boldsymbol{r}) c_{n\boldsymbol{K}}(t) c^*_0(t) + c.c. \end{aligned} \tag{3.34}$$

If the steady-state population $c_{n\boldsymbol{K}}(t \to \infty)$ is used and if we assume that the response to changes in the electromagnetic field $\boldsymbol{E}$ is instant and linear, it is then possible to obtain an approximation for the average dielectric constant of a QD due to the exciton in it:

$$\boldsymbol{P}(\boldsymbol{r}, \omega) = \frac{e^2 \boldsymbol{p}_{cv}}{\hbar(\omega_{n\boldsymbol{K}} - \omega) m_0 \omega^2_{n\boldsymbol{K}}} \Psi_{n\boldsymbol{K}}(\boldsymbol{r}, \boldsymbol{r}) \int \Psi^*_{n\boldsymbol{K}}(\boldsymbol{r}', \boldsymbol{r}') \boldsymbol{p}_{cv} \cdot \boldsymbol{E}(\boldsymbol{r}', \omega) \,\mathrm{d}\boldsymbol{r}' + c.c. \tag{3.35}$$

where it was assumed that $c_0(t) \approx 1$ which is true for weak excitation.

Still assuming linear dependence on $\boldsymbol{E}$ and also that $\boldsymbol{p}_{cv}$ is constant or always in the same direction as the electromagnetic field, we can do the following approximation to get the dielectric constant for a quantum dot of radius R:

$$\boldsymbol{D}(\boldsymbol{r},\omega) = \varepsilon_\infty \boldsymbol{E}(\boldsymbol{r},\omega) + \boldsymbol{P}(\boldsymbol{r},\omega) = \varepsilon_{QD}(\boldsymbol{r},\omega)\boldsymbol{E}(\boldsymbol{r},\omega) \tag{3.36}$$

which gives

$$\varepsilon_{\mathrm{QD}}(\boldsymbol{r},\omega) = \varepsilon_\infty \left(1 + \sum_{n\boldsymbol{K}} \frac{2\omega_{LT}}{\omega_{n\boldsymbol{K}} - \omega} \frac{\sin\alpha_{n\boldsymbol{K}}}{\alpha_{n\boldsymbol{K}}}\right) \tag{3.37}$$

where $\alpha_{n\boldsymbol{K}} = \pi|\boldsymbol{r}-\boldsymbol{a}|/R$. $\omega_{LT} = e^2 p_{cv}^2/\pi\varepsilon_\infty \hbar\omega_{n\boldsymbol{K}}^2 m_0^2 a_B^3$. The transverse-longitudinal exciton splitting ω_{LT} is a measure of the strength of the exciton's influence on light entering the quantum dot, and the reason for the name will be elaborated below.

The expression for a bulk semiconductor's dielectric constant is quite similar [19], only lacking the $\sin(\alpha_{n\boldsymbol{K}})/\alpha_{n\boldsymbol{K}}$ spatial dependence.

The complex QD dielectric constant $\varepsilon_{QD}(\omega) = \varepsilon' + i\varepsilon''$ is plotted in figure 3.1, where typical values for a CdSe QD of 2 nm radius have been used: $\hbar\omega_{LT} = 50$ meV, $\hbar\omega_{QD}$=2.23 eV, $\gamma = 10$ meV and $\varepsilon_\infty = 12$.

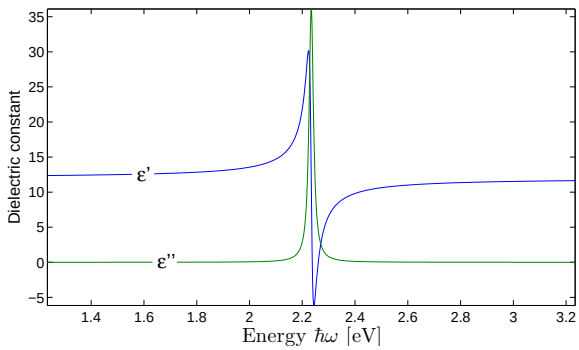

Figure 3.1: Complex dielectric constant of the model QD

3.3 Exciton-polaritons

Having obtained the dielectric constant of a QD due to excitons inside the QD, an important question to be addressed is what happens to the light which enters the quantum dot.

It is helpful to use the idea of exciton-polaritons, which are the strongly coupled combination of the exciton and the photons in the EM field around it. The strong coupling can be understood by considering the interdependencies in the QD system. The exciton population dynamics depends on the electromagnetic field, and the EM

field inside the quantum dot is strongly determined by the dielectric constant of the QD which exhibits a strong variation around the exciton's resonance frequency.

As a starting point for understanding the effect of exciton-polaritons, we consider the effect of the excitonic modification of the dielectric constant on the electromagnetic field in a bulk material. This is done by using the complex dielectric constant $\varepsilon(\omega)$ in the wave equation for the electromagnetic field:

$$\boldsymbol{k} \times (\boldsymbol{k} \times \boldsymbol{E}(\boldsymbol{r}, \omega)) - \frac{\omega^2}{c^2}\epsilon(\omega)\boldsymbol{E}(\boldsymbol{r}, \omega) = 0 \tag{3.38}$$

We can decompose the E field into two fields, a *transverse* field perpendicular to $\boldsymbol{k}$ and a *longitudinal* field parallel to $\boldsymbol{k}$, and obtain two equations to solve.

For the transverse part we have:

$$\left(k^2 - \frac{\omega^2}{c^2}\epsilon(\omega)\right)\boldsymbol{E}(\boldsymbol{r}, \omega) = 0 \tag{3.39}$$

which directly yields the dispersion relation

$$k^2 = \frac{\omega^2}{c^2}\epsilon(\omega) \tag{3.40}$$

For the longitudinal part we get:

$$\frac{\omega^2}{c^2}\epsilon(\omega) = 0 \tag{3.41}$$

which is satisfied only if $\epsilon(\omega, \boldsymbol{k}) = 0$, which is possible if the dielectric function is expanded with nonlocal terms that depend on k.

The dispersion diagram for the transverse part is shown in figure 3.2 together with the bare light and exciton dispersions given by $\omega = ck/\sqrt{\epsilon_\infty}$ and $\omega = \omega_0 + \hbar k^2/2m^*$ respectively.

What this shows is that there is a strong interaction between photons and excitons, visible as an anticrossing. Notably there is no solution for a narrow range of energies close to the exciton resonance frequency ω_0 called the stop band, which means no light can be transported in that range due to the excitons' interaction with the light. This is visible as an increased reflectance in the stop band.

This treatment was for bulk materials, without decay mechanisms and nonlocality. With decay and nonlocality the stop band is not complete, causing the sample to have varying and imperfect reflection and absorption in the stop band. In quantum dots the general picture is modified somewhat - the idea of using the wave equation to determine light transport properties is no longer valid due to the small size - it is no longer the *transport* properties that matter but rather the *scattering* properties. However the basic effect still remains as the polarization will create a local strongly varying effective dielectric constant which affects the photons entering the QD. This leads to increased reflectivity of QDs close to the exciton resonance energy, which has been observed experimentally with very good fits to theoretical calculations [21].

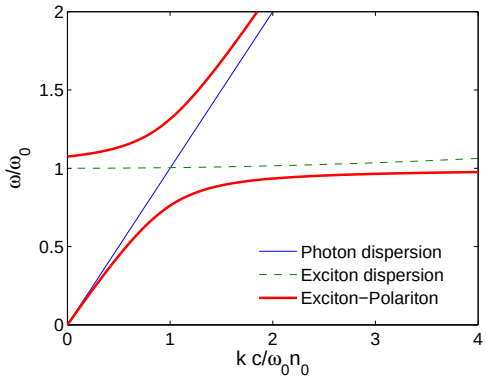

Figure 3.2: The dispersion diagram for photons, ground-state exciton and the exciton-polariton

3.4 Effect on the Stokes shift

In paper I we investigated the effect of the exciton polariton on the absorption spectrum of a QD and the Stokes shift - the energy difference between the absorption peak and the luminescence peak of a quantum dot. We can roughly assume that the luminescence peak always occurs at the exact exciton energy as it is very likely between the ground electron and hole states, while the absorption can be between higher-lying states and be affected by the polarization of the ground state which modifies the effective dielectric constant of the QD.

In the paper, a numerical approach using the Finite Difference Time Domain method was taken, but here to make the physics more clear and build a solid foundation for future work, here the expression for the electric field magnitude inside a quantum dot is derived using elementary electrostatics.

Let the quantum dot be a perfect sphere of radius R. Assume that the illumination is uniform in space (outside of the QD) as the difference in the typical QD size and illumination wavelengths is large. We can then describe the external electromagnetic field as constant $\boldsymbol{E}_{ext}(\omega) = \boldsymbol{E}_0$.

The dielectric constant is the average of the local QD dielectric constant $\varepsilon_{QD}(\boldsymbol{r}, \omega)$ taken over the QD volume from eq. 3.37, with a decay parameter γ included:

$$\varepsilon_{QD}(\omega) = \epsilon_\infty \left(1 - \frac{6\omega_{LT}}{\pi^2(\omega_{QD} - \omega + i\gamma)}\right) \tag{3.42}$$

The exact epression of the field inside a dielectric sphere is a classic problem [20], here we will only demonstrate a few of the steps.

We have a sphere, radius R, of a linear dielectric with dielectric constant ϵ_{in} embedded in another infinite medium with dielectric constant ϵ_{out}.

To find the E field, we first solve Laplace's equation for the electric potential V in spherical coordinates, $\nabla^2 V = 0$. As the general solutions to the Laplace equation in spherical coordinates are spherical harmonics, we write the specific solutions for the E field inside and outside the QD as a sum of spherical harmonics (without the ϕ dependence since the problem is really cylindrically symmetric - we have one major axis determined by the external field's direction and the problem is symmetric around that vector):

$$V_{in} = \sum_{l=0}^{\infty} \left(A_l r^l + \frac{B_l}{r^{l+1}} \right) P_l(\cos(\theta)) \tag{3.43}$$

$$V_{out} = \sum_{l=0}^{\infty} \left(C_l r^l + \frac{D_l}{r^{l+1}} \right) P_l(\cos(\theta)) \tag{3.44}$$

θ here is the angle between the point of interest and the external field's E direction. P_l are Legendre polynomials. The boundary conditions determines the variables A, B, C, D.

As the potential should be finite at $r = 0$ inside the QD, all B_l values are zero. The far field's potential should be $-E_0 r \cos(\theta)$, so $C_1 = -E_0$ (as $P_1(x) = x$) and all other C_l values are zero.

The remaining constants are determined by the boundary conditions at $r = R$:

$$\text{Tangential E:} \quad \varepsilon_{out} E_{out}^{\perp}\Big|_R - \varepsilon_{QD} E_{in}^{\perp}\Big|_R = \sigma_f \tag{3.45}$$

$$\text{Continuous potential V:} \quad V_{in}\Big|_R = V_{out}\Big|_R \tag{3.46}$$

where σ_f is the free charge density at the surface. As a semiconductor has no free charges except those photoexcited (which are very few and mostly contained in the center of the QD, away from the surface R), we can write $\sigma_f = 0$. By $E = -\nabla V$ we can write the tangential E boundary condition in terms of the potential V:

$$\varepsilon_{out} \frac{\partial V_{out}}{\partial r}\Big|_R = \varepsilon_{QD} \frac{\partial V_{in}}{\partial r}\Big|_R \tag{3.47}$$

Condition 3.46 gives:

$$\sum_{l=0}^{\infty} A_l R^l P_l(\cos(\theta)) = -E_0 R \cos(\theta) + \sum_{l=0}^{\infty} D_l R^{-(l+1)} P_l(\cos(\theta)) \tag{3.48}$$

Condition 3.47 becomes:

$$\varepsilon_{out} \sum_{l=0}^{\infty} A_l l R^{l-1} P_l(\cos(\theta)) = -E_0 \cos(\theta) - \sum_{l=0}^{\infty} D_l (l+1) R^{-(l+2)} P_l(\cos(\theta)) \tag{3.49}$$

As the legendre polynomials are orthonormal, each terms in both conditions has to be equal for every index l. The only solution for $l \neq 1$ is $A_l = D_l = 0$. For $l = 1$,

the solution is

$$A_1 = \frac{-3\varepsilon_{out}}{\varepsilon_{in} + 2\varepsilon_{out}} E_0 \tag{3.50}$$

$$D_1 = \frac{\varepsilon_{in} - \varepsilon_{out}}{\varepsilon_{in} + 2\varepsilon_{out}} E_0 R^3 \tag{3.51}$$

Thus the potential inside the QD is

$$V_{in}(r,\theta) = A_1 r\cos(\theta) = \frac{-3\varepsilon_{out}}{\varepsilon_{in} + 2\varepsilon_{out}} E_0 r\cos(\theta) \tag{3.52}$$

To get the E field, we use $E = -\nabla V$. As the potential is cylindrically symmetric, we can elegantly write $z = r\cos(\theta)$, set the external field as $E_0\hat{\boldsymbol{z}}$ and use the ∇ operator in cartesian coordinates instead of the more complicated spherical or cylindrical coordinates, $\nabla = (\partial_x, \partial_y, \partial_z)$. We end up with the result

$$\boldsymbol{E}_{in} = \frac{-3\varepsilon_{out}}{\varepsilon_{in} + 2\varepsilon_{out}} \boldsymbol{E}_0 \tag{3.53}$$

Having an expression for the E field inside a QD, and the dielectric constant of the QD ($\varepsilon_{QD}(\omega)$ from 3.37), it is now possible to investigate how the optical field inside the QD varies around the QD excitation wavelength, shown in figure 3.3.

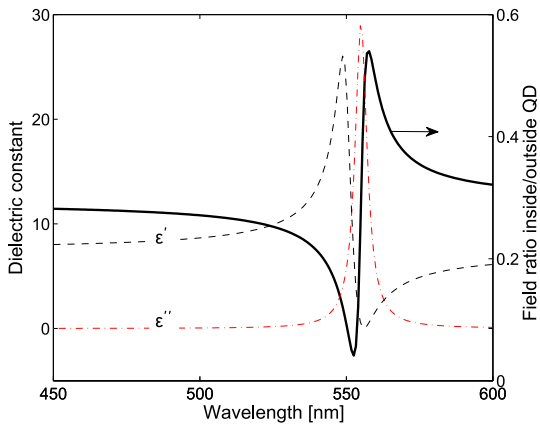

Figure 3.3: The complex dielectric constant of the 3.4 nm diameter QD studied in paper I, and the resulting ratio of electromagnetic field amplitude inside/outside the QD

We see that when $\varepsilon_{in} < \varepsilon_{out}$, the E field is increased inside the QD due to accumulation, so when the optical densities of the QD and the environment are swapped (environment denser than QD), the field inside the QD is stronger. This effect is familiar from classical electrodynamics.

What is novel is the idea of including this effect in the modeling of the shape of the absorption spectrum which due to the suppression of the ground state exciton absorption reveals an easily observed shift between absorption and luminescence peaks, which hitherto has usually required complicated explanations relying on band structure effects.

Thus when the QD dielectric constant is high, which occurs for energies below the exciton resonance energy, the QD can be expected to scatter more of the electromagnetic field so less light enters the QD to be absorbed. For higher energies, the dielectric constant can become small or even negative, which leads to an increased amount of light inside the QD. There is an energy difference of roughly $\hbar\gamma$ between the resonance energy and the smallest value of the dielectric constant, indicating a possible contribution to the Stokes shift.

The typically observed absorption of a QD ensemble is, as was remarked in chapter 2.4, smoothed due to phonon interactions and size distribution. It can be calculated from the exciton energies E_i of a QD by summing Lorentzian peaks,

$$A_{abs}(\hbar\omega) = \sum_i \frac{A_i}{\pi} \frac{\Gamma}{(\hbar\omega - E_i)^2 + \Gamma^2}$$

To demonstrate the modification to the measured absorption spectrum, we take the calculated energies and absorption strengths from paper I, for a 3.4 nm diameter CdSe QD with ground state transition at 555 nm, and use the electric field ratio $|\boldsymbol{E}_{in}/\boldsymbol{E}_0|$ given by eq. 3.53 to modulate the absorption spectrum. The results are shown in fig. 3.4, which clearly shows an enhanced peak shape for the absorption when the QD field is modulated by the exciton polariton. The peak emphasizes the second transition level instead of the ground state transition, which may contribute to the observed Stokes shift.

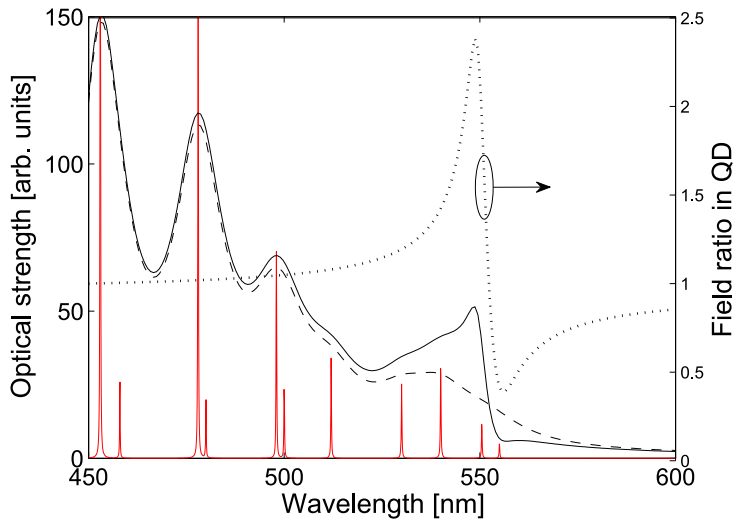

Figure 3.4: Calculated absorption spectrum, without (dashed) and with (whole) the exciton-polariton modulation (dotted curve, normalized values). The QD energy levels and their relative optical strengths are shown as sharp peaks.

Chapter 4

Surface Plasmon Polaritons

Having obtained both qualitative and quantitative understanding of the electrooptical properties of semiconductor quantum dots, we now turn our attention to metal nanostructures.

Metals are materials with a high number of free electrons - this property causes the various phenomena we usually associate with metals: good conductivity and high reflectivity. The high number of free electrons allow us to skip quantum effects since the many electrons lead to very narrow energy spacings, less than $k_B T$, so classical electrodynamics can be used for the metal throughout this thesis.

We can qualitatively consider the metal as consisting of a plasma (the free electrons as a gas of free charges) in an ionic background (the atoms). Exciting the plasma will lead to waves in the electron density which can be quantized by introducing the quasiparticle *plasmon*. The plasmons will again interact with a surrounding electromagnetic field, so the concept of plasmon-polariton is again useful just as it was for the exciton-polariton.

The plasma model, if extended with collisions with ions, defects, phonons, etc, modeled phenomenologically by a collision rate γ_0, leads to the Drude-Sommerfeld model of a metal's dielectric constant:

$$\varepsilon(\omega) = \varepsilon_\infty - \frac{\omega_p^2}{\omega^2 + i\gamma_0\omega} \tag{4.1}$$

where ω_p is the plasma frequency, $\omega_p = \sqrt{ne^2/\varepsilon_0 m^*}$, in which n is the density of the free electrons and m^* is the average effective mass. The collision rate γ_0, often called the relaxation parameter, can be obtained from measurements of the direct-current conductivity σ through $\gamma_0 = ne^2/\sigma m^*$.

This model, albeit very simple, manages to describe many metals very well. One example is shown in figure 4.1, where the real and imaginary parts of the dielectric constant of silver is presented in the visible and near-visible wavelength range. When considering shorter wavelengths, interband contributions take on a larger role which is not included in the Drude model.

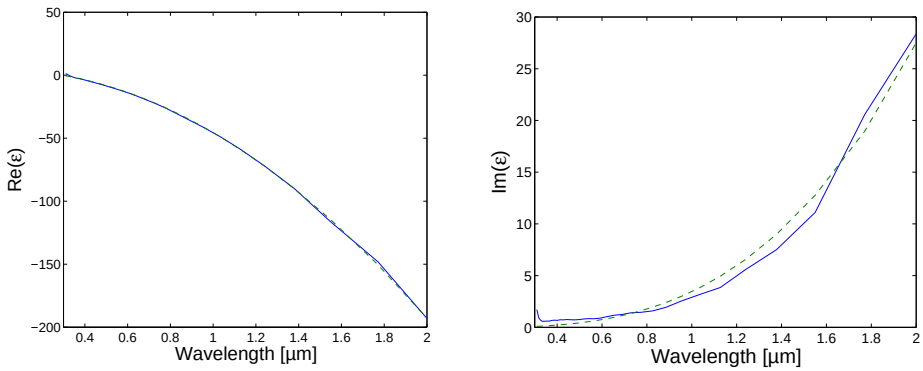

(a) Real part (b) Imaginary part

Figure 4.1: The dielectric constant of silver, measured data taken from[22], with a fit using the Drude model (dashed line)

For this reason and to be able to better model the imaginary part, it is common to use the multipole Drude-Lorentz material model, which can exhibit multiple resonances:

$$\varepsilon(\omega) = \varepsilon_\infty \left(1 + \sum_{p=1}^{P} \frac{f_p \omega_p}{\omega_p^2 + 2i\omega\gamma_p - \omega^2}\right) \tag{4.2}$$

In order to use a multipole Drude-Lorentz model a nonlinear fitting to experimental values is performed. When a narrow range is considered, a single-pole fit is often sufficient, but for wider ranges, 4-pole models are common [23].

There is no need to treat actual electrons or plasmons in calculation models to observe plasmonic effects - all that's needed is the effect the electrons have on the material's properties, described by the dielectric constant.

The wave equation leads to a dispersion relation for the plasmon-polariton which depends on the dielectric constant, just like it did for the exciton-polariton. Solving the Maxwell equations at a planar interface between a metal with a frequency-dependent dielectric constant $\varepsilon_m(\omega)$ and a dielectric with ε_d, the dispersion relation for surface plasmons propagating on the interface when coupled to transverse magnetic (TM) illumination is:

$$k_{sp} = \frac{\omega}{c}\sqrt{\frac{\varepsilon_d \varepsilon_m(\omega)}{\varepsilon_d + \varepsilon_m(\omega)}} \tag{4.3}$$

If the sign of the metal's dielectric constant $\epsilon_m(\omega)$ is the opposite to that of the dielectric, then the square root will be larger than one - the surface plasmon polariton (SPP) mode momentum is greater than that of light propagating in the dielectric.

Metals usually have negative dielectric constants over a broad range of optical frequencies as clearly seen in figure 4.1a, while all dielectrics have positive-valued ε_d. This means that many metal-dielectric interfaces are able to host SPP waves.

The limit where $k_{sp} \to \infty$ represents the stationary surface plasmon mode which does not have a polaritonic character as the surface plasmons do not behave like propagating light, instead being more like stationary states (solved by the Laplace equation instead of the wave equation)

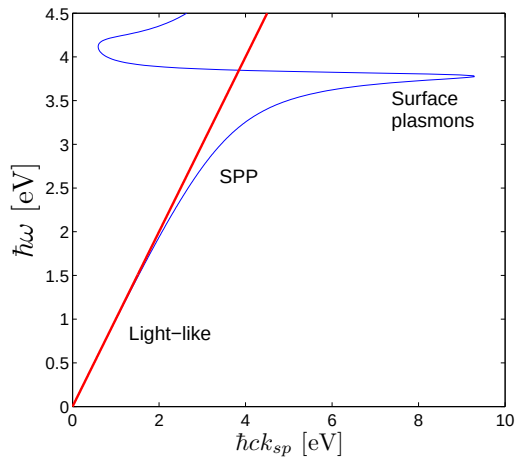

Figure 4.2: The surface plasmon polariton dispersion, using the Drude fit to silver presented in figure 4.1

Momentum conservation prevents incident light from coupling into the SPP modes unless the momentum mismatch is compensated, or exceeded (upon which some of the momentum energy is lost to heat)

The most common and popular way to overcome this is to use a prism in either the Otto[24] or Kretschmann[25] configurations, both of which utilize evanescent fields created when total internal reflection is achieved in the prism. The evanescent fields have the necessary momentum to couple with SPPs on a metal-air interface close to the prism surface.

Another approach is to use a grating or a periodic surface feature in order to achieve quasi-phase matching with the additional momentum provided by the lattice period:

$$\boldsymbol{k}_{spp} = \boldsymbol{k}_{||} + \frac{2m\pi}{L_x}\boldsymbol{u}_x + \frac{2n\pi}{L_y}\boldsymbol{u}_y \tag{4.4}$$

where $\boldsymbol{u}_x, \boldsymbol{u}_y$ are the unit vectors of the reciprocal lattice of the periodic surface feature, L_x and L_y are the grating real space primitive lattice constants. The integers m, n indicates the plasmon mode and direction. $\boldsymbol{k}_{||}$ is the photon wave vector parallel to the surface on which SPPs are supposed to be created.

Successful coupling into plasmons is visible as a strong decrease in reflection in all three methods of excitation. As the SPP resonance is sensitive to the values of the dielectric constant of the dielectric medium, a change in the dielectric constant of the environment will cause significant shifts of the SPP resonance which is used directly in SPP resonance biosensors [26].

4.1 Local field enhancement

The solutions for the SPP $\boldsymbol{E}$ fields decay exponentially with the distance from the interface and are bound, they are not radiative modes - thus most metal surfaces exhibit a strong *local* field that is normally not observed except when using Scanning Near-field Optical Microscopy probes (SNOM).

The light captured by the metal nanostructure will be confined to a quite small volume, not much larger than the nanostructure itself, which concentrates the energy gained from the incident field. The localised field is thus often much stronger than the incident field, which has led to the widespread use of the Surface-Enhanced Raman Spectroscopy (SERS) method [27] where the Raman spectrum response of a molecule on a nanostructured metal surface is extremely strongly enhanced. The enhancement factor can be as high as 10^{10} [28]. Many other nonlinear effects like Second-Harmonic Generation [29] and Sum Frequency Generation [30] are also strongly enhanced, as the nonlinear effects depend strongly on the electromagnetic field intensity.

The strong local field also enhances the fluorescence of dye molecules and quantum dots near the metal surface, by modifying the fluorescence decay rate. [31][32]

A popular method to achieve high local field enhancements is to create bowtie antennas - two triangles facing each other, like a bowtie. The sharp corners enhance the SPP field, resulting in a very high-intensity field between the two triangles. This has allowed single-molecule detection.

4.2 Metal nanoparticle arrays

When considering the interaction of light with a metallic nanoparticle, typically the nanoparticle is sufficiently small for the light to be able to penetrate into the whole nanoparticle and be treated as uniform throughout the nanoparticle. The electric field inside the metal shifts all the free electrons in one direction, building up a charge at the surface at one side of the nanoparticle. At the other side the depletion of electrons leads to a positive charge, which attracts the electrons back. Together with the external electromagnetic field, this restoring force creates a collective oscillation throughout the entire particle which can be amplified by resonant interaction of the external illumination with the nanoparticle. This oscillation makes the particle behave like a dipole, with both local and radiative fields. This dipole makes the particle absorb strongly light with wavelengths close to the resonance.

The strongly wavelength-dependent properties of metal nanoparticles have long been used phenomenologically, for making brightly coloured glasses for church windows.

By placing multiple nanoparticles close to each other, the plasmons in each nanoparticle can couple with the plasmons in the other nanoparticle by the Coulomb dipole-dipole interaction. This has led to very sensitive sensors for particle-particle distances [33] and linear nanoparticle chains as SPP waveguides [34] [35] [36].

Auguie [37] demonstrated both theoretically and experimentally that an ordered two-dimensional lattice of nanoparticles with period $L > 2\pi/k_{spp}$ will, due to diffractive effects, efficiently couple light into the planar array. The drawback is that the distances involved are quite large, in the order of a few hundreds of nanometers, so no local field enhancement effect nor particle-particle interactions will be observable - the plasmons supported by the nanoparticles are standalone particle plasmons whose resonance only depends on the particle geometry, material and the interplay with the array diffraction modes.

For larger nanoparticles where retardation effects become important, the nanoparticles can be arranged in particular patterns that supports multiple plasmonic modes which interfere, leading to asymmetric Fano resonances which are very sensitive to changes in the environment [38][39][40].

4.3 Subwavelength Hole Arrays

Ebbesen et al. [41] found in 1998 that a thin silver film perforated with a regular hole array exhibited a few long-wavelength transmission peaks that were much higher than classical aperture theory allowed for. This phenomenon, called Extraordinary Optical Transmission (EOT), generated a lot of interest due to the possibility of improving the light transmission through electrical contacts for sensors and displays [45].

There are many differing explanations of the EOT effect, but the widely held view is that it is caused by the resonant excitation of SPPs on the metal surface which guides the energy through the holes [42]. This theory was supported by a strong angular dependence measured in Ebbesen's experiments, which fits with the plasmon description as plasmonic excitation is very strongly angle-dependent.

The relationship between EOT and SPPs is also clearly marked by the fact that the enhanced transmission peaks appear at the SPP wavelengths [43]

$$\lambda_{SPP} = \frac{P}{i^2 + j^2}\sqrt{\frac{\epsilon_m \epsilon_d}{\epsilon_m + \epsilon_d}} \tag{4.5}$$

where i, j are the grating modes, and P is the grating period. The idea of plasmon transport being responsible was verified by Grupp et al. [44], who did measurements on a metal film with a single hole in a lattice grating of dimples. A dimple grating allows the incident radiation to couple with the grating plasmon mode, which is

tunneled through the hole. Their results showed an EOT effect at long wavelengths, confirming the theory.

The possibility of utilizing this effect for improving the photoresponse of a quantum dot infrared photodetector has garnered a great deal of attention. Typically a roughly fourfold increase in the photocurrent is observed [46] [47] [48] usually attributed to the the local field enhancement and the EOT. In paper III, we showed that a more important reason for the increase is the improved light-matter coupling in the QDs due to the classical diffraction by the periodic hole array which bends the light, not the local field effect which is small at the typical position of the quantum dot layer in a QDIP structure. Quantum dots are commonly assumed to be isotropically absorbing at any angle due to the simplified concept of an artificial atom, but epitaxial quantum dots of the kind often used in QDIPs are more like flattened cylinders, which introduces an angular dependence so the diffraction caused by the hole array is the main reason of the increased observed photocurrent.

A high-index dielectric grating would therefore have a similar effect, without the strong absorption of metals. However, due to the usual device design of QDIPs with metallic contact layers on the top, patterning the top metal contact is a simple and cost-effective way to increase the photocurrent and sensitivity of the QDIP.

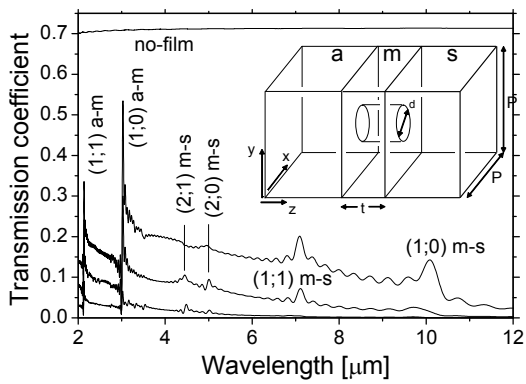

Figure 4.3: Transmission coefficient of a metal thin film with 3 μm period $1\mu m$ diameter hole array calculated by FDTD. Inset: schematic geometric grating structure. Plasmon $(i; j)$ modes are labelled, "a-m" and "m-s" denote air-metal and metal-semiconductor interfaces. From low to high transmission curves: $d = 800$, 1200, 1600 nm; The curve at about 0.7 denotes the case without any metal film.

Chapter 5

Solving the Maxwell Equations

In this chapter the Finite Difference Time Domain (FDTD) method for solving the Maxwell equations is described.

FDTD is preferable to analytical approaches like the one in chapter 3.4, as it can handle arbitrary geometry, for which plasmonic effects are difficult to calculate, and the time-based approach allows us to insert the exciton dynamics later in chapter 6, which is impossible to do for the popular Discrete Dipole Approximation (DDA) method which is a frequency-domain method.

There are typically two main approaches to solving the Maxwell equations - *frequency-domain* and *time-domain* methods. In frequency-domain methods such as the plane-wave methods, DDA, FDFD (Finite-difference frequency-domain) and FEM (finite-element method) approaches, the frequency of the source excitation is a fixed value so that the source is always turned on, and the steady-state spatial distribution of the electromagnetic field is obtained from a large matrix equation. The issue with this approach is that often the spectrum is of more interest than the distribution of fields, so repeated calculations over a range of frequencies are necessary, and the exciton dynamics require a time-dependent approach to be used as Fourier transforming the exciton Bloch equations is very complicated so treating the problem in the time domain is easier.

In time-domain methods, the source excitation can be either fixed-frequency or pulsed. The wave propagation in space is updated step-wise over time, and usually a discrete Fourier transform of the data is carried out to obtain spectral information.

If the incident wave is a broadband pulse which covers a wide range of frequencies then the Fourier transform of the output by a single calculation can yield the system response over the wide range of frequencies - thereby saving a considerable amount of calculation time.

Seeing the wave propagate through the structure can be very helpful in understanding how the system responds to external stimuli, which in part explains why time-domain methods are popular. Another reason is that FDTD is particularly

easy to implement in code.

The main drawback is that the spectral resolution of the Discrete Fourier Transform depends on the number of time steps, so to observe small details more steps are needed, which can make FDTD calculations computationally expensive. The discretization can also introduce some errors, but in practice these are usually smaller than experimental errors.

5.1 The Maxwell equations

First we consider the equations to solve, the *macroscopic* Maxwell equations in differential form. The macroscopic version of the equations are used when dealing with electromagnetic fields inside matter instead of in free space, by defining auxiliary fields $\boldsymbol{D}$ and $\boldsymbol{H}$ - the electric displacement field and magnetizing field, respectively.

If we stipulate that there are no free charges and no magnetic currents, as we do not study charged structures and do not use magnetic materials, then we can write the equations as:

$$\nabla \cdot \boldsymbol{D} = 0 \tag{5.1}$$

$$\nabla \cdot \boldsymbol{B} = 0 \tag{5.2}$$

$$\nabla \times \boldsymbol{E} = -\frac{\partial \boldsymbol{B}}{\partial t} \tag{5.3}$$

$$\nabla \times \boldsymbol{H} = \frac{\partial \boldsymbol{D}}{\partial t} + \boldsymbol{J} \tag{5.4}$$

The displacement field $\boldsymbol{D}$ here is related to the electric field $\boldsymbol{E}$ by $\boldsymbol{D} = \varepsilon_0 \boldsymbol{E} + \boldsymbol{P}$, where $\boldsymbol{P}$ is the polarization field. In linear materials whose polarization responds instantly and linearly on the electric field, we have $\boldsymbol{P} = \varepsilon_0 \chi \boldsymbol{E}$ and $\boldsymbol{D} = \varepsilon \boldsymbol{E}$ where $\varepsilon = \varepsilon_0(1 + \chi) = \varepsilon_0 \varepsilon_r$ in which we have defined the relative dielectric constant ε_r.

Similarly, the magnetizing field can be written as $\boldsymbol{H} = \mu \boldsymbol{B} = \mu_0 \mu_r \boldsymbol{B}$, where μ_r is the relative permeability.

The two divergences $\nabla \cdot \boldsymbol{D}$ and $\nabla \cdot \boldsymbol{B}$ are trivial and not used in the calculations. The componentwise x, y, z expansions of the rotational terms, without the current density $\boldsymbol{J}$ which will be added later, are:

$$\frac{\partial H_x}{\partial t} = \frac{1}{\mu}\left(\frac{\partial E_y}{\partial z} - \frac{\partial E_z}{\partial y}\right) \tag{5.5}$$

$$\frac{\partial H_y}{\partial t} = \frac{1}{\mu}\left(\frac{\partial E_z}{\partial x} - \frac{\partial E_x}{\partial z}\right) \tag{5.6}$$

$$\frac{\partial H_z}{\partial t} = \frac{1}{\mu}\left(\frac{\partial E_x}{\partial y} - \frac{\partial E_y}{\partial x}\right) \tag{5.7}$$

$$\frac{\partial E_x}{\partial t} = \frac{1}{\varepsilon}\left(\frac{\partial H_z}{\partial y} - \frac{\partial H_y}{\partial z}\right) \tag{5.8}$$

$$\frac{\partial E_y}{\partial t} = \frac{1}{\varepsilon}\left(\frac{\partial H_x}{\partial z} - \frac{\partial H_z}{\partial x}\right) \tag{5.9}$$

$$\frac{\partial E_z}{\partial t} = \frac{1}{\varepsilon}\left(\frac{\partial H_y}{\partial x} - \frac{\partial H_x}{\partial y}\right) \tag{5.10}$$

5.2 The FDTD method

The basic idea is to evaluate the curl terms in the Maxwell equations numerically by finite differences on a staggered grid, which solves numerical issues with coupled equations on the same grid point and gives second-order accuracy. Additionally, the $\boldsymbol{E}$ and $\boldsymbol{H}$ fields are calculated in a leapfrog manner with the time of $\boldsymbol{H}$ being $\Delta t/2$ later than the $\boldsymbol{E}$ field [49].

The $\boldsymbol{E}$ and $\boldsymbol{H}$ components are placed at different points in the lattice grid's volume cubes, see figure 5.1.

We use an uniform rectangular grid with integer indices (i, j, k) to denote the spatial positions $(i\Delta x, j\Delta y, k\Delta z)$, where $\Delta x, \Delta y, \Delta z$ are the spatial increments in the x, y, z axes, respectively. The time is discretized as $t = n\Delta t$, so that n is the time step number.

Consider a function $u(\boldsymbol{r}, t)$ in space and time. If it is discretized as $u(i\Delta x, j\Delta y, k\Delta z, n\Delta t)$ then we can use central differences to discretize the first derivative in space and time. The spatial derivative over x becomes, with step size $\Delta x/2$:

$$\frac{\partial u(i\Delta x, j\Delta y, k\Delta z)}{\partial x} = \frac{u^n_{i+1/2,j,k} - u^n_{i-1/2,j,k}}{\Delta x} + O[(\Delta x)^2] \tag{5.11}$$

and in time, with step size $\Delta t/2$:

$$\frac{\partial u(i\Delta x, j\Delta y, k\Delta z)}{\partial t} = \frac{u^{n+1/2}_{i,j,k} - u^{n-1/2}_{i,j,k}}{\Delta t} + O[(\Delta t)^2] \tag{5.12}$$

Using these approximations on eqs. 5.5-5.10 yields the following discretized expressions:

$$H_x^{n+1/2}(i,j,k) = H_x^{n-1/2}(i,j,k) + \frac{\Delta t}{\mu(i,j,k)}\left[\frac{E_y^n(i,j,k+1/2) - E_y^n(i,j,k-1/2)}{\Delta z} - \frac{E_z^n(i,j+1/2,k) - E_z^n(i,j-1/2,k)}{\Delta y}\right] \tag{5.13}$$

$$H_y^{n+1/2}(i,j,k) = H_y^{n-1/2}(i,j,k) + \frac{\Delta t}{\mu(i,j,k)}\left[\frac{E_z^n(i+1/2,j,k) - E_z^n(i-1/2,j,k)}{\Delta x} - \frac{E_x^n(i,j,k+1/2) - E_x^n(i,j,k-1/2)}{\Delta z}\right] \tag{5.14}$$

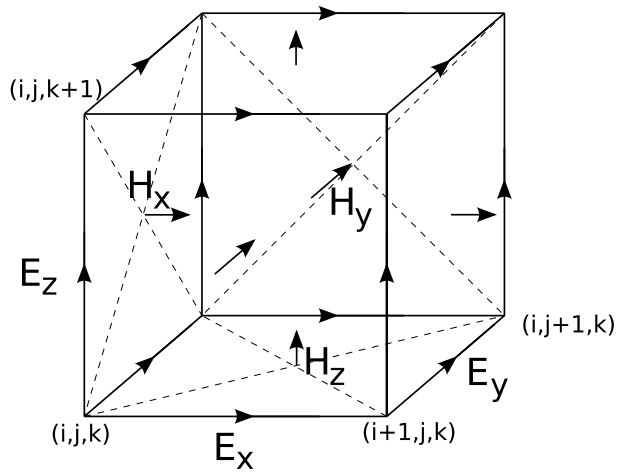

Figure 5.1: The Yee lattice, which staggers the E and H field components in space. The E components are placed at the edges and the H components are placed at face centers

$$H_z^{n+1/2}(i,j,k) = H_z^{n-1/2}(i,j,k) + \frac{\Delta t}{\mu(i,j,k)} \left[\frac{E_x^n(i,j+1/2,k) - E_x^n(i,j-1/2,k)}{\Delta y} - \frac{E_y^n(i+1/2,j,k) - E_y^n(i-1/2,j,k)}{\Delta x} \right] \tag{5.15}$$

$$E_x^{n+1}(i,j,k) = E_x^n(i,j,k) + \frac{\Delta t}{\varepsilon(i,j,k)} \left[\frac{H_z^{n+1/2}(i,j+1/2,k) - H_z^{n+1/2}(i,j-1/2,k)}{\Delta y} - \frac{H_y^{n+1/2}(i,j,k+1/2) - H_y^{n+1/2}(i,j,k-1/2)}{\Delta z} \right] \tag{5.16}$$

$$E_y^{n+1}(i,j,k) = E_y^n(i,j,k) + \frac{\Delta t}{\varepsilon(i,j,k)} \left[\frac{H_x^{n+1/2}(i,j,k+1/2) - H_x^{n+1/2}(i,j,k-1/2)}{\Delta z} - \frac{H_z^{n+1/2}(i+1/2,j,k) - H_z^{n+1/2}(i-1/2,j,k)}{\Delta x} \right] \tag{5.17}$$

$$E_z^{n+1}(i,j,k) = E_z^n(i,j,k) + \frac{\Delta t}{\varepsilon(i,j,k)} \left[\frac{H_y^{n+1/2}(i+1/2,j,k) - H_y^{n+1/2}(i-1/2,j,k)}{\Delta x} - \frac{H_x^{n+1/2}(i,j+1/2,k) - H_x^{n+1/2}(i,j-1/2,k)}{\Delta y} \right] \tag{5.18}$$

5.3 Boundary conditions

When performing a computer simulation of a system there is usually a small limited region of interest within an open unbounded system. Due to time and cost constraints, only a small part of the open region can be included in the simulation. Simply setting zero derivatives does not work as the E and H fields depend on each other in a nontrivial way which would yield spurious reflections if Neumann boundary conditions are used. This indicates that a more sophisticated boundary condition is necessary in order to reduce spurious reflections.

A quite simple yet efficient method is the Uniaxial Perfectly Matched Layers (UPML) method [50]. Conceptually one can think of this method as defining an absorbing region of space in which the spatial coordinates are substantially stretched. The stretching of the coordinates makes it possible to absorb more of the electromagnetic fields propagating in the region. If the material is defined to be gradually more absorbent closer to the simulation volume edges, there is no sharp reflecting interface - the PML is then a kind of impedance matching where the material is also strongly absorbent in order to avoid reflections from the actual edges of the simulation volume.

We define a complex stretching factor

$$s_{x,y,z} = 1 + \frac{\sigma_{x,y,z}}{i\omega\varepsilon} \tag{5.19}$$

Here $\sigma_{x,y,z}$ is the UPML's "conductivity" which determines the absorptivity of the UPML medium. It is graded across the UPML in order to avoid sharp discontinuities which would cause reflections.

In the frequency domain, the stretched curl equations can be written as

$$\nabla \times \boldsymbol{H} = i\omega\varepsilon\bar{s}\boldsymbol{E} \tag{5.20}$$

$$\nabla \times \boldsymbol{E} = -i\omega\mu\bar{s}\boldsymbol{H} \tag{5.21}$$

where the tensor $\bar{s}$ is

$$\bar{s} = \begin{bmatrix} \frac{s_y s_z}{s_x} & 0 & 0 \\ 0 & \frac{s_x s_z}{s_y} & 0 \\ 0 & 0 & \frac{s_x s_y}{s_z} \end{bmatrix} \tag{5.22}$$

Directly transforming the frequency-domain equations into time domain would, due to the multiple ω factors, lead to complicated expressions involving convolution which are costly to perform. A better approach is to use a modified electric displacement field $\tilde{\boldsymbol{D}}$ to obtain an auxiliary ordinary differential equation.

We write

$$\tilde{D}_x = \varepsilon\frac{s_z}{s_x}E_x; \qquad \tilde{D}_y = \varepsilon\frac{s_x}{s_y}E_y; \qquad \tilde{D}_z = \varepsilon\frac{s_y}{s_z}E_z \tag{5.23}$$

If these constitutive relations are used instead of $\boldsymbol{E}$ in 5.20, we get

$$\left(\frac{\partial H_z}{\partial y} - \frac{\partial H_y}{\partial z}\right) = i\omega s_y \tilde{D}_x \tag{5.24}$$

$$\left(\frac{\partial H_x}{\partial z} - \frac{\partial H_z}{\partial x}\right) = i\omega s_z \tilde{D}_y \tag{5.25}$$

$$\left(\frac{\partial H_y}{\partial x} - \frac{\partial H_x}{\partial y}\right) = i\omega s_x \tilde{D}_z \tag{5.26}$$

As the relationships are simpler and linearly dependent on ω with some of the complexity hidden in the $\tilde{\boldsymbol{D}}$ variables, it is now possible to perform the inverse Fourier transform $i\omega f(\omega) \rightarrow (\partial/\partial t) f(t)$, yielding

$$\left(\frac{\partial H_z}{\partial y} - \frac{\partial H_y}{\partial z}\right) = \frac{\sigma_y}{\varepsilon} D_x + \frac{\partial}{\partial t} D_x \tag{5.27}$$

$$\left(\frac{\partial H_x}{\partial z} - \frac{\partial H_z}{\partial x}\right) = \frac{\sigma_z}{\varepsilon} D_y + \frac{\partial}{\partial t} D_y \tag{5.28}$$

$$\left(\frac{\partial H_y}{\partial x} - \frac{\partial H_x}{\partial y}\right) = \frac{\sigma_x}{\varepsilon} D_z + \frac{\partial}{\partial t} D_z \tag{5.29}$$

The relations in eqs. 5.23 can be transformed into the time domain too:

$$\frac{\partial D_x}{\partial t} + \frac{\sigma_x}{\varepsilon} D_x = \varepsilon \left(\frac{\partial E_x}{\partial t} + \frac{\sigma_z}{\varepsilon} E_x\right) \tag{5.30}$$

$$\frac{\partial D_y}{\partial t} + \frac{\sigma_y}{\varepsilon} D_y = \varepsilon \left(\frac{\partial E_y}{\partial t} + \frac{\sigma_x}{\varepsilon} E_y\right) \tag{5.31}$$

$$\frac{\partial D_z}{\partial t} + \frac{\sigma_z}{\varepsilon} D_z = \varepsilon \left(\frac{\partial E_z}{\partial t} + \frac{\sigma_y}{\varepsilon} E_z\right) \tag{5.32}$$

From this the $\boldsymbol{E}$ field can be obtained. The magnetization $\boldsymbol{H}$ is treated in a similar manner.

The discretization in time and space is carried out just as for the main FDTD method, yielding four update terms, two for the electric field and two for the magnetic field. For the electric field there are one for $\boldsymbol{D}$ from the curl of $\boldsymbol{H}$, and one for $\boldsymbol{E}$ from $\boldsymbol{D}$.

In a computer implementation, the PML and $\boldsymbol{E}, \boldsymbol{H}$ field calculations can be merged by setting $\sigma_{x,y,z} = 0$ outside of the PML.

The other boundaries can be periodic, for example in the x axis:
$\boldsymbol{E}(x = 0, y, z) = \boldsymbol{E}(x = L_x, y, z)$ and similarly for $\boldsymbol{H}$. This makes it possible to simulate a planar slice of a nanostructured material by imposing periodic boundary conditions in two axes and allowing the light to propagate in the third axis.

5.4 Dispersive materials

As were discussed in the previous chapters, materials can have a frequency-dependent dielectric constant. The treatment of the dielectric constant in the FDTD method

assumes that it is constant, so there is a need to extend the method to frequency-dependent materials too.

This is done by utilizing the current density $\boldsymbol{J}$ due to polarization. Since the frequency-dependent polarization of metals is classical and complicated to obtain, the dielectric constant is instead fitted to a model with multiple Lorentzian poles:

$$\varepsilon(\omega) = \varepsilon_\infty \left(1 + \sum_{p=1}^{P} \frac{A_p}{\omega_p^2 + 2i\omega\delta_p - \omega^2}\right) \tag{5.33}$$

This gives three fitting parameters for each pole: the strength A_p, the pole frequency ω_p and the damping factor δ_p.

The frequency-dependent current density is then, for a pole p:

$$\boldsymbol{J}_p(\omega) = \frac{i\omega\epsilon_0 A_p \omega_p^2}{\omega_p^2 + 2i\omega\delta_p - \omega^2} \boldsymbol{E}(\omega) \tag{5.34}$$

Fourier transforming this is relatively simple:

$$\omega_p^2 \boldsymbol{J}_p(t) + 2\delta_p \frac{\partial}{\partial t}\boldsymbol{J}_p(t) + \frac{\partial^2}{\partial t}\boldsymbol{J}_p(t) = A_p \frac{\partial}{\partial t}\boldsymbol{E}(t) \tag{5.35}$$

Discretizing this in time, using central differences yields:

$$\boldsymbol{J}_p^{n+1/2} = a_p \boldsymbol{J}_p^n + b_p \boldsymbol{J}_p^{n-3/2} + c_p(\boldsymbol{E}^n - \boldsymbol{E}^{n-1}) \tag{5.36}$$

with

$$a_p = \frac{2 - \omega_p^2 \Delta t^2}{1 + \delta_p \Delta t}, \tag{5.37}$$

$$b_p = \frac{\delta_p \Delta t - 1}{1 + \delta_p \Delta t} \tag{5.38}$$

$$c_p = \frac{A_p \Delta t}{1 + \delta_p \Delta t} \tag{5.39}$$

To use this $\boldsymbol{J}$, the $\boldsymbol{E}$ fields need to be updated. Eq. 5.4 becomes:

$$\nabla \times \boldsymbol{H}^{n+1/2} = \varepsilon_0 \varepsilon_\infty \frac{\partial}{\partial t}\boldsymbol{E}(t) + \sum_{p=1}^{P} \boldsymbol{J}_p(t) \tag{5.40}$$

Discretizing this in time (but not space, for clarity) results in:

$$\boldsymbol{E}^{n+1} = \hat{\boldsymbol{E}}^{n+1} + \frac{\Delta t}{\varepsilon_0 \varepsilon_\infty} \left(\sum_{p=1}^{P} \boldsymbol{J}_p^{n+1/2}\right) \tag{5.41}$$

where $\hat{\boldsymbol{E}}$ is the $\boldsymbol{E}$ field from the nondispersive FDTD calculation steps in eqs. (5.16)-(5.18) which are to be updated.

The complete FDTD algorithm can now be described. At each time step n, the following steps are performed in order:

- Calculate nondispersive $\boldsymbol{E}^n$, including PML
- Update $\boldsymbol{E}^n$ with $\boldsymbol{J}^{n-1/2}$
- Calculate $\boldsymbol{J}^{n+1/2}$
- Update sources
- Calculate $\boldsymbol{H}^{n+1/2}$, including PML
- Perform a Discrete Fourier Transform step
- Increment the step index n

Chapter 6

Exciton-Plasmon Interactions

In this chapter we consider the effects of solving both the Maxwell and Schrödinger equations simultaneously, when the equations are coupled.

As both exciton-polaritons and surface plasmon-polaritons have resonances in the visible or the near-UV/IR regions, strong modifications of the local electromagnetic field, strong absorption, easily adjusted properties, to combine both materials in the same system has generated a lot of interest.

The enhanced near field close to metal surfaces can be absorbed by QDs and other semiconductor structures, enhancing the absorption of the composite system - a trait of great interest for photodetectors [51] and solar cells [52][53].

Enhanced absorption can also lead to increased photoluminescence in materials consisting of both QDs and metal structures [54]. The local field enhancement close to metal surfaces has been shown to reduce the blinking effect observed in small colloidal QDs [55], although the exact reason of the blinking suppression is not yet known.

The main emphasis has often been on modifying the emission properties of QDs, by amplifying the electromagnetic field in QDs which by the Purcell effect leads to a reduction in spontaneous decay rates and an increase in luminescence but QDs have also been used to modify plasmonic systems by the strong variation of the dielectric constant in QDs, with applications in modulators [56].

Excitons in quantum wells have also been coupled to plasmonic grating structures, with observed polariton anticrossing behaviour of the resonance peaks in the angle-dependent reflectivity spectrum [57][58] at low temperatures - but the weaker excitonic response of quantum wells prevents practical use in room-temperature operation, which is possible with quantum dots.

In chapter 3 the exciton dynamics were partly obtained in order to find a dielectric constant. The model used to obtain the QD dielectric constant was for standalone quantum dots without any interactions with the environment and assumed a constant steady illumination. This model is likely to be invalid when metal structures supporting plasmon modes with a resonance in the same frequency range

as the exciton are placed close to the QDs.

These effects are mainly unidirectional - they are either plasmons modifying the exciton properties or the exciton modifying the plasmonic properties. To observe a real bidirectional interaction between both the exciton and plasmon the nanostructures need to be of similar sizes.

In the weak coupling regime, both the exciton wavefunction and plasmon mode are unperturbed - the only coupling is in the population dynamics through the interaction between the exciton dipole and the plasmon fields. The main effect seen in this regime is the modification of the excitation lifetime (decay) - both by the Purcell effect and by modification of the stimulated emission. Energy transfers due to the long-range Coulomb interaction is also possible.

In the strong coupling regime, the exciton wavefunction and/or the plasmon mode can be perturbed which cause resonance energy splitting and shifts. The energy of the coupled system oscillates between the metallic and the semiconductor parts, causing a Rabi oscillation in the population. If the QD is of similar size as the metal structure, then the strong change in the dielectric constant of the QD can affect the plasmon mode, which provides a tractable pathway to observing the strong coupling regime.

The exciton-plasmon interaction is often visible as an antiresonance, or a Fano resonance, due to the sharp resonance of the QD ($\gamma \approx 0.1 - 10$ meV) within an usually broader ($\gamma \approx 100$ meV) plasmon resonance profile, demonstrated pictorially in figure 6.1

Without a strong interaction, the composite optical properties is usually a superposition of the two resonances, although often the QD resonance can be difficult to observe due to its relatively weaker and narrower peak to that of the plasmon resonance.

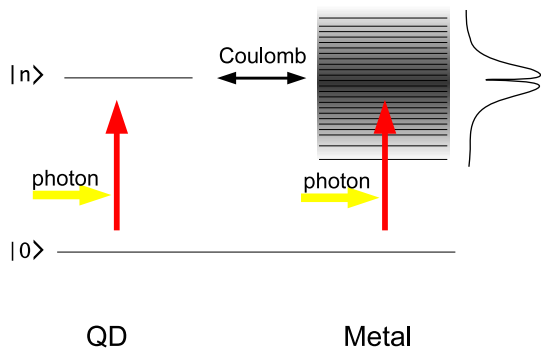

Figure 6.1: Illustration of the exciton-plasmon interaction, their resonance widths and the antiresonance which appears in strongly interacting systems

Generally three approaches can be taken to calculate the properties of a coupled exciton-plasmon system. The first is to assume a weak unidirectional effect and

calculate the plasmon and exciton responses separately only using the $|\boldsymbol{E}|$ field to determine the exciton response to the given electric field. In paper III and IV, this approach was used as the difference in size between the QDs and the metal hole array structure, and the distance between the QDs and the metal surface, were sufficiently large enough for the QD exciton-polariton to have a negligible influence on the plasmonic properties.

The second, which can be used if both nanostructures are spherical nanoparticles, is to use particle plasmons and treat the structures as dipoles and just study dipole-dipole interactions without considering the plasmon electric field distribution. This approach is popular for obtaining the coupled exciton-plasmon interaction and is detailed briefly below in chapter 6.2.

The third is to do a fully coupled Maxwell-Schrödinger calculation, which we have done in papers II and V.

6.1 The fully coupled Maxwell-Schrödinger method

If the metal surface is not simple enough to be treated as a dipole, a full FDTD or FEM calculation has to be performed in order to obtain the plasmon response. The exciton dynamics can be inserted in the time stepping of the FDTD method if the polarization $\boldsymbol{P}$ due to the exciton is used in the $\boldsymbol{E}$ field calculation.

A popular approach is to use density matrices to describe the population dynamics of a system so this approach is adapted here as well.

We consider the photodynamics of excitons in a quantum dot by a multi-level model with the vacuum ground state (no excitons) and pairs of one electron and one hole (excitons) which may have different energies. For now we ignore biexcitons, triexcitons, etc - the model is fully extendable to those extended pairings which is mostly observed at low temperatures and high quality samples and so can be ignored for most calculations aimed for practical devices.

Label the vacuum ground state as $|0\rangle$ with zero energy and the exciton states as $|n\rangle$ with energy $\hbar\omega_n$, $n = [1, N]$ where the total number of possible exciton states N depends on the QD size and material parameters (usually only the lowest few levels matter, often just the first exciton state is sufficient). The hamiltonian is then

$$H = \sum_{n}^{N} \hbar\omega_n |n\rangle\langle n| + H_I \tag{6.1}$$

The dipole interaction Hamiltonian H_I is:

$$H_I = -\sum_{n} \left(\int \boldsymbol{d}(\boldsymbol{r}) \cdot E(\boldsymbol{r}, t) \, \mathrm{d}^3 r \right) |n\rangle\langle 0| + h.c. \tag{6.2}$$

where "h.c." signifies hermitian conjugate. The exciton dipole-moment operator is the same as in chapter 3, and $E(\boldsymbol{r}, t)$ is the electric field inside the quantum dot. A very common approximation is to assume a constant E field inside the QD and move it outside the integral but here this approximation is not used.

For the following steps, we use a shorter notation by putting the dipole moment integral into just one variable μ_{n0}:

$$H_I = -\sum_n \mu_{n0}|n\rangle\langle 0| + h.c. \tag{6.3}$$

Now the density matrix ρ is introduced:

$$\rho = \sum_{mn} \rho_{mn}|m\rangle\langle n| \tag{6.4}$$

For example, for a two-state system (vacuum + one exciton level) we have:

$$\rho = \rho_{00}|0\rangle\langle 0| + \rho_{11}|1\rangle\langle 1| + \rho_{10}|1\rangle\langle 0| + \rho_{01}|0\rangle\langle 1| + ... \tag{6.5}$$

Additional terms of e.g. couplings to the environment, coupling to other nanostructures, etc., may be added but it is common to neglect those and focus at just the active parts.

As we neglect other reservoirs, all of the non-excited population must be in the ground state. We thus have the relation $\rho_{00} = 1 - \sum_n \rho_{nn}$

All Coulomb-type interactions with metallic structures (which do not have distinct energy levels with long lifetimes and is thus not well-suited for treating using density matrices) are done through the dipole interaction hamiltonian, and the E field on the metal structures due to the QD polarization, both of which are calculated using FDTD.

The dynamics of the various states is governed by the master equation (Liouville equation):

$$i\hbar\frac{\partial\rho}{\partial t} = [H, \rho] - i\Gamma(\rho) \tag{6.6}$$

where Γ is the relaxation matrix, usually approximated as ρ_{nm}/τ_{nm} where τ_{nm} describes the lifetime and broadening of that state/transition.

We can get equations of motion for the various states by premultiplying with $\langle n|$ and postmultiplying with $|m\rangle$ on both sides:

$$i\hbar\frac{\partial\rho_{nm}}{\partial t} = \langle n|[H, \rho]|m\rangle - \sum_{kl} i\Gamma_{nm,kl}\rho_{kl} \tag{6.7}$$

Expanding the $\langle n|[H, \rho]|m\rangle$ matrix elements leads to the population dynamics equations:

$$i\hbar\frac{\partial\rho_{nn'}}{\partial t} = \hbar(\omega_n - \omega_{n'})\rho_{nn'} + \mu_{0n'}\rho_{n0} - \mu_{n0}\rho_{0n'} \tag{6.8}$$

$$i\hbar\frac{\partial\rho_{n0}}{\partial t} = \hbar\omega_n\rho_{n0} - \mu_{n0}\rho_{00} + \sum_{n'} \mu_{n'0}\rho_{nn'} \tag{6.9}$$

We do not bother with obtaining other equations since they all can be found from $\rho_{nn'}$ and ρ_{n0}, through $\rho_{n'n} = \rho^*_{nn'}$ and $\rho_{00} = 1 - \sum_n \rho_{nn}$.

The dipole matrix element is $\mu_{nm} = \langle n| \left(\int \boldsymbol{d}(\boldsymbol{r}) \cdot E(\boldsymbol{r},t) \mathrm{d}^3 r \right) |m\rangle$, already evaluated earlier in chapter 3.

The polarization is given by the operator $\hat{\boldsymbol{P}}(t) = \sum_n \boldsymbol{d}_{0n}\rho_{n0}(t) + h.c.$. We find $\rho_{n0}(t)$ by solving the population dynamics equations. The dipole matrix element $\boldsymbol{d}_{0n} = \langle n|e\boldsymbol{r}|0\rangle$ was obtained in chapter 3: $\boldsymbol{d}_{0n} = -ie\boldsymbol{p}_{cv}\psi^*_{n,\boldsymbol{K}}(\boldsymbol{r},\boldsymbol{r})/m_0\omega_n$, where the exciton envelope function $\Psi_{n,\boldsymbol{K}}$ is

Summing up the results of this section, we have the following key equations: For the density matrix (population of the various states $0, n, n'$:

$$i\hbar\frac{\partial\rho_{nn'}}{\partial t} = \hbar(\omega_n - \omega_{n'})\rho_{nn'} + \mu^*_{n'0}\rho_{n0} - \mu_{n0}\rho^*_{n'0} \tag{6.10}$$

$$i\hbar\frac{\partial\rho_{n0}}{\partial t} = \hbar\omega_n\rho_{n0} - \mu_{n0}\rho_{00} + \sum_{n'}\mu_{n'0}\rho_{nn'} \tag{6.11}$$

with the dipole matrix element

$$\mu_{n0} = \frac{e}{im_0\omega_n}\boldsymbol{p}_{cv} \cdot \int \psi^*_{n,\boldsymbol{K}}(\boldsymbol{r},\boldsymbol{r})\boldsymbol{E}(\boldsymbol{r},t)d^3r \tag{6.12}$$

where the electric field $\boldsymbol{E}(\boldsymbol{r},t)$ is obtained from the FDTD calculation step.

For the polarization the following expression is used:

$$\boldsymbol{P}(\boldsymbol{r},t) = \sum_n \frac{e}{m_0\omega_n}\rho_{n0}(t)\boldsymbol{p}_{cv}\psi^*_{n,\boldsymbol{K}}(\boldsymbol{r},\boldsymbol{r}) + h.c. \tag{6.13}$$

We couple the QD polarization into the FDTD calculations by:

$$\boldsymbol{J}(\boldsymbol{r},t) = -\frac{\partial\boldsymbol{P}(\boldsymbol{r},t)}{\partial t} = \sum_n \frac{e}{m_0\omega_n}\frac{\partial\rho_{n0}(t)}{\partial t}\boldsymbol{p}_{cv}\psi^*_{n,\boldsymbol{K}}(\boldsymbol{r},\boldsymbol{r}) + h.c. \tag{6.14}$$

Care has to be taken in order to avoid self-interactions, which can be especially problematic in array structures. Since the $\boldsymbol{J}$ field is continuously updated, it is possible to calculate two fields in FDTD: one for the total system $\boldsymbol{E}_{tot}$and one for just the QD $\boldsymbol{E}_{QD}$, without any other interactions. This second field is used to remove any self-interactions, $\boldsymbol{E} = \boldsymbol{E}_{tot} - \boldsymbol{E}_{QD}$. In periodic systems, PML is used for the calculation of the $\boldsymbol{E}_{QD}$ field's boundaries to avoid spurious interactions with copies of itself.

To do a combined FDTD+density matrix calculation, the following steps are performed at each time step:

- Calculate $\boldsymbol{E}^n_{tot}$ field, with $\boldsymbol{J}^{n-1/2}$ from both the QD and the metal structures
- Calculate $\boldsymbol{E}^n_{QD}$ field, from the $\boldsymbol{J}^{n-1/2}$ field from the QD in the previous step
- Get the E field to use in calculations, $\boldsymbol{E}^n = \boldsymbol{E}^n_{tot} - \boldsymbol{E}^n_{QD}$

- Calculate the change in the QD exciton population ρ_{nn} and ρ_{n0} using time-discretized versions of eqs. 6.10 and 6.11 and $\boldsymbol{E}^n$.
- Calculate $\boldsymbol{J}^{n+1/2}$ from $\partial\rho_{n0}/\partial t$, inside the QD, using eq. 6.14
- Calculate $\boldsymbol{J}^{n+1/2}$ using the auxiliary differential equation, in the metal structures
- Update sources, $\boldsymbol{H}$, perform Fourier transform, increment step index n, just as for normal FDTD

6.2 Interactions in nanoparticle systems

Before discussing the results of the full coupled Maxwell-Schrödinger calculations, the most common approach to obtain exciton-plasmon interactions is here detailed so that the differences and advantages/disadvantages of each method is understood.

The exciton-plasmon interaction is mostly studied for pairs of nanoparticles, one metal and one semiconductor, assuming that both can be represented simply by its dipole and that the $\boldsymbol{E}$ field is constant over the QD/MNP. With these assumptions, the full FDTD calculation can be skipped, allowing the use of a similar treatment as in chapter 3.4.

The near field around a dipole with the dipole moment $\boldsymbol{p}$ is

$$\boldsymbol{E} = \frac{3\boldsymbol{n}(\boldsymbol{n}\cdot\boldsymbol{p}) - \boldsymbol{p}}{4\pi\varepsilon_0\varepsilon_r r^3} \tag{6.15}$$

where $\boldsymbol{n} = \boldsymbol{r}/|\boldsymbol{r}|$ is the unit direction vector to the point to calculate the E field at.

The electromagnetic field inside the QD can be decomposed into three parts:

One due to the external field:

$$\boldsymbol{E}_1 = \frac{\epsilon_{out}}{\epsilon_{eff}(\omega)}\boldsymbol{E}_0 \tag{6.16}$$

where $\varepsilon_{eff}(\omega) = (\varepsilon_{QD}(\omega) + 2\varepsilon_{out})/3$ is the effective QD dielectric constant, which includes the exciton-polariton modification to the absorption spectrum discussed in chapter 3.4.

Another due to the Coulomb interaction with the charges on the metal nanoparticle induced by the external field, for which we use eq. 6.15.

The dipole moment of a metal nanosphere of radius R_m with dielectric constant ϵ_m in an uniform electric field $\boldsymbol{E}_0$ in a media with dielectric constant ϵ_{out} is:

$$\boldsymbol{p} = 4\pi\varepsilon_0\varepsilon_{out}R_m^3\frac{\varepsilon_m(\omega) - \varepsilon_{out}}{\varepsilon_m(\omega) + 2\varepsilon_{out}}\boldsymbol{E}_0 \tag{6.17}$$

This yields

$$\boldsymbol{E}_2 = \frac{\varepsilon_{out}R_m^3}{d_{Q-M}^3}\frac{\varepsilon_m(\omega) - \varepsilon_{out}}{\varepsilon_m(\omega) + 2\varepsilon_{out}}\frac{3\boldsymbol{n}(\boldsymbol{n}\cdot\boldsymbol{p}) - \boldsymbol{p}}{4\pi\varepsilon_0\varepsilon_{eff}(\omega)r^3} \tag{6.18}$$

where d_{Q-M} is the distance between the two nanoparticles and R_{MNP} is the MNP radius.

The final contribution comes from the charges on the MNP induced by the QD itself.

$$\boldsymbol{E}_3 = \frac{\varepsilon_{out} R_m^3}{d_{Q-M}^6} \frac{\varepsilon_m(\omega) - \varepsilon_{out}}{\varepsilon_m(\omega) + 2\varepsilon_{out}} \frac{3\boldsymbol{n}(\boldsymbol{n} \cdot \boldsymbol{p}_{QD}) - \boldsymbol{p}_{QD}}{4\pi\varepsilon_0 \varepsilon_{eff}^2(\omega) r^3} \tag{6.19}$$

where $\boldsymbol{p}_{QD} = \boldsymbol{\mu}_{n0}\rho_{n0} + h.c.$, obtained earlier. Notably the d_{Q-M}^6 distance dependence makes E_3 very small when the distance between the particles are large, indicating that the exciton-plasmon interactions require very small distances.

Using these expressions for the total electromagnetic field inside the QD, together with the Bloch equations 6.10 and 6.11, it is possible to set up a system of equations which can be solved if a few approximations are done.

Using this method a few groups have investigated a rich set of physical phenomena associated with the exciton-plasmon interaction.

Artuso and Bryant showed that the simple system of a QD and a metal nanoparticle can still exhibit three different characteristic scattering spectra depending on the strength of the exciton-plasmon interaction - an asymmetric Fano shape of the scattering spectrum, a double-peaked Fano shape or a bistable system which depends on the initial exciton population [59]

The Fano interference's effect on the absorption spectrum can be strong enough to make the QD+metal structure transparent in a very narrow frequency range [61] [62]. The closely related slow light phenomenon has also been theoretically predicted for a QD+metal nanoparticle composite system, wherein the group velocity is considerably slowed down [63].

Nonradiative Förster Energy Transfers (FRET) either between the metal and QD or between two metal nanoparticles can be assisted by a QD [64], by the Coulomb interaction between nanoparticles of different sizes, offering a great deal of control of the optical power flow in nanostructures.

Exciton-plasmon interactions with spins in quantum dots tuned by magnetic fields has been studied in [65] which shows that the changes in the extinction spectrum and energy level shifts due to exciton-plasmon interactions can be further tuned by strong magnetic fields.

The issue with the approach used in these works is that it assumes that the nanoparticles can always be treated as a whole, with an uniform E field inside. This breaks down when the geometry is not as simple, when the size of the nanoparticles is large enough and when multiple nanoparticles are present, for which multipole effects have to be accounted for [66]

The effects of a quantum dot between two elongated metal nanoparticles were studied by Wu [62] using FDTD with a simple steady-state frequency-dependent dielectric constant for the QD, and by Savasta using the dipole-dipole model [60]. A QD-induced near-total transparency was found within the plasmonic absorption peak, which was explained in terms of a coupled oscillator model - the addition of a QD which alone would have absorbed the light at its resonant frequency led

to interactions of the QD dipole with the surrounding particle plasmon dipoles, quenching the absorption of both at the QD resonance frequency.

The dielectric constant of a QD can be expected to be different when coupled to a plasmon system as the exciton polarization will be interacting with the plasmon so to take the steady-state approximation of a lone QD without metal surfaces close by, like in the derivation of eq. 3.37, is not likely to present the full picture of the exciton-plasmon interaction.

In paper V, we have used the coupled FDTD + density matrix approach to calculate a similar QD+metal dimer structure, in addition to a few oligomeric structures which adds more metal surfaces for absorbing the light in order to observe the efficiency of the exciton-polariton-induced reduction in absorption. Similar structures with larger metal nanoparticles have shown complex Fano interferences due to retardation effects [38] but it is not present for the small sizes of nanoparticles studied here - the idea of using oligomeric structures is here merely to study the effects of enhanced exciton-plasmon interactions in the presence of additional metal surfaces and a more robust plasmon mode.

We found that with our more detailed description of the QD resonance, shown for a metal nanoparticle dimer + QD structure in figure 6.2, the QD-induced transparency is not as strong as demonstrated by Wu et al., which we attribute to our less idealized model of the QD population, more localised exciton wavefunction and a slower optical response.

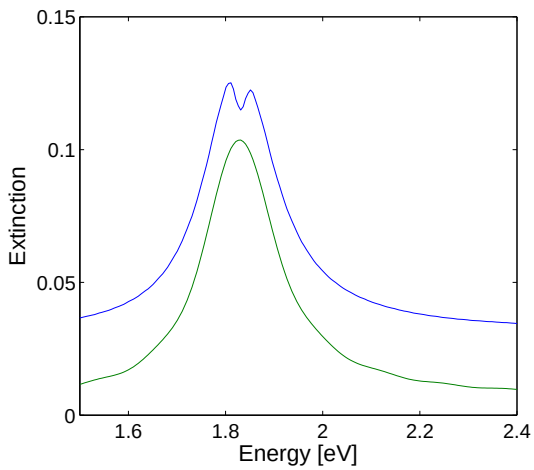

Figure 6.2: The plasmonic peak in the extinction, and the exciton-induced dip. The curve for the exciton-plasmon interaction result has been shifted upwards for clarity

Chapter 7

Summary of the papers and outlook

In paper I, the modification of the absorption profile by QDs were calculated using FDTD in order to partially explain the Stokes shift between absorption and luminescence peaks. In this work, the steady-state approximation to the excitonic dielectric constant was used in the usual FDTD method without the density matrix approach described in chapter 6. In chapter 3, a simplified theoretical calculation is presented, which was done by me after the paper was published, for an unpublished followup work.

In paper II, an early and simple version of the density matrix approach for the exciton population time evolution was added to the FDTD software, and used to study the QD excitation under very intense femtosecond laser illumination, for which several common approximations used in the group's past works could be expected to break down. It was shown that the errors do not exceed 1%, if just one QD is studied. A few other approximations were also studied, like averaging the wavefunction over the whole QD, taking the ground state exciton population as constant, etc - all of which showed very small and acceptable errors. This shows that even commercial FDTD software without access to the source code can be used to simulate systems consisting of only QDs, as long as the QDs are in a moderately homogeneous environment. The effect of more complex environments is a topic that remains to be studied in the future.

In paper III, a QDIP structure featuring a thin metal film with holes was studied by FDTD, demonstrating the Extraordinary Optical Transmission effect and studying its application for improving the QDIP photocurrent. The QDs were not included in the FDTD calculation, due to the huge size difference between the metal structure and the QDs, so the optical properties of the QDs were obtained by a simple time-independent calculation using the average electric field at the position of QDs in the QDIP structure. Commonly the improved photocurrent is attributed to local field enhancements and/or the EOT effect but in this work we showed that the diffraction effects are more important as they allow for better coupling into hemispherical QDs with wide base which, unlike the overly idealized spheri-

cal model of a QD, has a directional dependence with slightly inferior absorption at normal incidence. The conclusion is that the observed photocurrent increases might also be observed in structures with high-index dielectric gratings instead of the metal thin film. As common QDIP designs already feature a metal top contact layer, patterning this layer is a simple and cost-effective way to increase the coupling of the electromagnetic field into QDs and thus increase the photocurrent of the device.

In paper IV, the FDTD method was used to study and contrast two different metal structures for concentrating the light inside QDIPs and reduce crosstalk between detector pixels - a metal grating and a concave hemispherical cavity. The concept of plasmons are not directly used, but plasmons do play an important role in supporting a strong local enhancement and controls the reflection properties of the grating structure in particular. The focusing effect of the concave structure was demonstrated to yield a stronger time-integrated photocurrent despite the long-lived local field in the grating structure which in comparison does not enhance the local field as strongly as the concave structure. Again, the QDs were not included in the calculation, due to the different length scales.

In paper V, the fully coupled density matrix FDTD calculation method was used to study the decrease in absorption that a QD can induce when present in a metal structure. This is to our knowledge the first time the full FDTD+density matrix approach has been used for the study of QD-plasmon interactions. We show that the QD-induced transparency demonstrated by simpler approaches show somewhat exaggerated results, likely due to the wavefunction collecting the exciton deeper inside the QD, away from the surface so that the exciton becomes screened by the QD static dipole constant, and a retarded response to the plasmonic oscillations. A few different oligomeric structures were studied, all of which demonstrate this effect quite clearly. An alternative view of the cause of the dip is considered, where the QD assists in tunneling the resonant energy through the planar structure.

The fully coupled density matrix FDTD code developed will in the future be used to study solar cell structures, biosensors, and other devices that consist of QDs and metal nanoparticles or other metal structures. As the method does not require the metal structures to be spherical, the possibilities for using the method to study complex structures are unlimited. The only restriction is the considerably higher calculational cost, but with advances in computing technology and parallelization this is not a big concern.

Bibliography

[1] M. Born, E. Wolf, *Principles of Optics: Electromagnetic Theory of Propagation, Interference and Diffraction of Light* (Pergamon Press, 1959)

[2] J. B. Pendry, D. Schurig, D. R. Smith, Science 312, 1780 (2006)

[3] U. Leonhardt, Science 312, 1777 (2006)

[4] V. G. Veselago, Sov. Phys.-Usp. 10, 509 (1968)

[5] E. O. Kane, J. Phys. Chem. Solids 1, 82 (1956)

[6] J. C. Phillips and L. Kleinman, Phys. Rev. 116, 287 (1959)

[7] Al. L. Efros and M. Rosen, Phys. Rev. B 15, 4843 (1996)

[8] D. O. Demchenko and L.-W. Wang, Phys. Rev. B 73, 155326 (2006)

[9] A. Bagga, P. K. Chattopadhyay, and S. Ghosh, Phys. Rev. B 74, 035341 (2006)

[10] J. M. An, A. Franceschetti, and A. Zunger, Nano Lett. 7, 2129 (2007)

[11] I. P. Ipatova, A. Yu. Maslov, and O. V. Proshina, Europhys. Lett. 53, 769 (2001)

[12] M. F. Frasco, N. Chaniotakis, Sensors 9, 7266 (2009)

[13] Z.-H. Chen, S. Hellström, Z.-J. Ning, Z.-Y. Yu, Y. Fu, J. Phys. Chem. C 115, 5286 (2011)

[14] P. Kukura, M. Celebrano, A. Renn, V. Sandoghar, Nano Lett. 9, 926 (2009)

[15] Y. Fu, T.-T. Han, Y. Luo, and H. Ågren, J. Phys. Condens. Matter 18, 9071 (2006)

[16] J. O. Dimmock, "Chapter 7 Introduction to the theory of exciton states in semiconductors", *S*emiconductors and Semimetals, vol.3, Academic press New York 1967, p.259-319.

[17] H. Haken, *Quantum Field Theory of Solids - An Introduction* (North-Holland Publishing Company, 1983)

[18] Y. Fu, M. Willander, and E. L. Ivchenko, Superlattices and Microstructures 27, 255 (2000)

[19] H. Haug and S. W. Koch, "Quantum Theory of the Optical and Electronic Properties of Semiconductors", 4th ed. (World Scientific, 2004)

[20] J. D. Jackson, "Classical Electrodynamics" (Wiley, 1962)

[21] Y. Fu, H. Ågren, L. Höglund, J. Y. Andersson, C. Asplund, M. Qiu and L. Thylen, Appl. Phys. Lett. 93, 183117 (2008)

[22] "Handbook of Optical Constants", Ed. E. D. Palik (Academic, 1985)

[23] F. Hao, P. Nordlander, Chem. Phys. Lett. 446, 115 (2007)

[24] A. Otto, Zeitschrift fur Physik, 216, 398 (1968)

[25] E. Kretschmann, H. Raether, Z. Naturf. A 23, 2135 (1968)

[26] B. Liedberg, C. Nylander, I. Lundström, Sens. Actuators, 4, 299 (1983)

[27] E. C. Le Ru, E. Blackie, M. Meyer, and P. G. Etchegoin, J. Phys. Chem. C 111, 13794 (2007)

[28] S. J. Oldenburg, S. L. Westcott, R. D. Averitt, N. J. Halas, J. Chem. Phys. 111, 4729 (1999)

[29] C. K. Chen, A. R. B. de Castro, and Y.-R. Shen, Phys. Rev. Lett. 46, 145 (1981)

[30] S. Baldelli, A. S. Eppler, E. Anderson, Y.-R. Shen, and G.A. Somorjai, J. Chem. Phys., 113, 5432 (2000)

[31] H. Kano and S. Kawata, Optics Lett. 21, 1848 (1996)

[32] T. Neumann, M.-L. Johansson, D. Kambhampati, W. Knoll, Advanced Functional Materials 12, 575 (2002)

[33] C. Tabor, R. Murali, M. Mahmoud, M. El-Sayed, J. Phys. Chem. A 113, 1946 (2009)

[34] M. Quinten, A. Leitner, J. R. Krenn, and F.R. Aussenegg, Opt. Lett. 23, 1331 (1998)

[35] J. R. Krenn, A. Dereux, J. C.Weeber, E. Bourillot, Y. Lacroute, J. P. Goudonnet, G. Schider, W. Gotschy, A. Leitner, F. R. Aussenegg, and C. Girard, Phys. Rev. Lett. 82, 2590 (1999)

[36] S. A. Maier, P. G. Kik, H. A. Atwater, S. Meltzer, E. Harel, B. E. Koel, and A. A. G. Requicha, Nature Mater. 2, 229 (2003)

[37] B. Augie and W. L. Barnes, Phys. Rev. Lett. 101, 143902 (2008)

[38] J. A. Fan, C. Wu, K. Bao, J. Bao, R. Bardhan, N. J. Halas, V. N. Manoharan, P. Nordlander, G. Shvets, and F. Capasso, Science 328, 1135 (2010)

[39] K. Bao, N. Mirin and P. Nordlander, Appl. Phys. A. 100, 333 (2010)

[40] N. Mirin, K. Bao, P. Nordlander, J. Phys. Chem. A. 113, 4028 (2009)

[41] T. W. Ebbesen, H. J. Lezec, H. F. Ghaemi, T. Thio, P. A. Wolff, Nature 391, 667 (1998)

[42] L. Martin-Moreno, F. J. Garcia-Vidal, H. J. Lezec, K. M. Pellerin, T. Thio, J. B. Pendry, T. W. Ebbesen, Phys. Rev. Lett. 86, 1114 (2001)

[43] H. F. Ghaemi, T. Thio, D. E. Grupp, T. W. Ebbesen, and H. J. Lezec, Phys. Rev. B 58, 6779 (1998)

[44] D. E. Grupp, H. J. Lezec, T. Thio, T. W. Ebbesen, Advanced Materials 11, 860 (1999)

[45] K. Tae Jin, T. Thio, T. W. Ebbesen, D. E. Grupp, and H. J. Lezec, Opt. Lett. 24, 256 (1999)

[46] R. V. Shenoi, D. A. Ramirez, Y. Sharma, R. S. Attaluri, J. Rosenberg, O. J. Painter, and S. Krishna, Proc. of SPIE 6713, 67130P (2007)

[47] C.-Y. Chang, H.-Y. Chang, C.-Y. Chen, M.-W. Tsai, Y.-T. Chang, S.-C. Lee, and S.-F. Tang, Appl. Phys. Lett. 91, 163107 (2007)

[48] S. C. Lee, S. Krishna, and S. R. J. Brueck, Optics Express 17, 23160 (2009)

[49] A. Taflove, S. C. Hagness, *"Computational Electrodynamics: The Finite-difference Time-domain Method"*, 2nd ed. (Artech House 2000)

[50] Z. S. Sacks, D. M. Kingsland, R. Lee, J. F. Lee, IEEE Trans. Antennas and Propagation 43, 1460 (1995)

[51] M. Jestl, I. Maran, A. Köck, W. Beinstingl, E. Gornik, Opt. Lett. 14, 719 (1989)

[52] D. M. Schaadt, B. Feng, and E. T. Yu, Appl. Phys. Lett. 86, 063106 (2005)

[53] A. J. Morfa, K. L. Rowlen, T. H. Reilly, M. J. Romero, and J. van de Lagemaat, Appl. Phys. Lett. 92, 013504 (2008)

[54] J. Lee, T. Javed, T. Skeini, A. O. Govorov, G. W. Bryant, and N. A. Kotov, Angew. Chem. 118, 4937 (2006)

[55] K. Ray, R. Badugu, and J. R. Lakowicz, J. Am. Chem. Soc. 128, 8998 (2006)

[56] D. Pacifici, H. J. Lezec, and H. A. Atwater, Nature Photonics 1, 402 (2007)

[57] P. Vasa, R. Pomraenke, S. Schwieger, Y. I. Mazur, V. Kunets, P. Srinivasan, E. Johnson, J. E. Kihm, D. S. Kim, E. Runge, G. Salamo, and C. Lienau, Phys. Rev. Lett. 101, 116801 (2008)

[58] S. Schwieger, P. Vasa, P. Pomraenke, C. Lienau, E. Runge, J. Phys.: Conf. Ser. 210, 012001 (2010)

[59] R. D. Artuso and G. W. Bryant, Nano Lett. 8, 2106 (2008)

[60] S. Savasta, R. Saija, A. Ridolfo, O. Di Stefano, P. Denti, and F. Borghese, ACS Nano 4, 6369 (2010)

[61] M. R. Singh, D. G. Schindel, and A. Hatef, Appl. Phys. Lett. 99, 181106 (2011)

[62] X. Wu, S. K. Gray, M. Pelton, Optics Express 18, 23633 (2010)

[63] Z. Lu and K.-D. Zhu, J. Phys. B: At. Mol. Opt. Phys. 42, 015502 (2009)

[64] S. M. Sadeghi, Appl. Phys. Lett. 99, 113113 (2011)

[65] A. O. Govorov, Phys. Rev. B, 82, 155322 (2010)

[66] J.-Y. Yan, W. Zhang, S. Duan, X.-G. Zhao, and A. O. Govorov, Phys. Rev. B 77, 165301 (2008)